EXPERIMENTAL INVESTIGATION OF TEARING FRACTURE IN SHEETS UNDER QUASI-STATIC LOADING

By

Michael L. Roach

B.S. Civil Engineering
Colorado State University, 1997

Submitted to the Department of Ocean Engineering and the Department of Civil and Environmental Engineering in partial fulfillment of the requirements for the degrees of

Naval Engineer in Naval Architecture and Marine Engineering
And
Master of Science in Civil and Environmental Engineering
At the
MASSACHUSETTS INSTITUTE OF TECHNOLOGY
June 2004

Signature of Author _____
The Department of Ocean Engineering and
The Department of Civil and Environmental Engineering
07 May 2004

Certified By _____
Tomasz Wierzbicki
Professor of Applied Mechanics, Department of Ocean Engineering
Thesis Supervisor

Certified By _____
Jerome J. Connor,
Professor of Civil and Environmental Engineering
Thesis Reader

Accepted By _____
Heidi M. Nepf
Associate Professor of Civil and Environmental Engineering
Chairman, Departmental Committee on Graduate Studies

Accepted By _____
Michael Triantafyllou
Professor of Ocean Engineering
Chairman, Departmental Committee on Graduate Studies

EXPERIMENTAL INVESTIGATION OF TEARING FRACTURE IN SHEETS UNDER QUASI-STATIC LOADING

By

Michael L. Roach

Submitted to the Department of Ocean Engineering and
The Department of Civil and Environmental Engineering
On 09 May 2004, in partial fulfillment of the requirements for the degrees of

Naval Engineer in Naval Architecture and Marine Engineering
and
Master of Science in Civil and Environmental Engineering

ABSTRACT

Although there has been interest in the behavior of metal plates under blast and projectile loading for many years, definitive open-source analysis has only been recently forthcoming. This analysis is most often in the form of scaled recreations of the dynamic blast event, or "live fire" tests. New developments in methods of recreating blast and projectile induced plate failure using a quasi-static approach provide possible, accurate, alternatives to the cumbersome and expensive live fire test.

This research endeavors to develop an accurate, quasi-static method of recreating the petalling phase of blast and projectile failure in metal sheets, based on a modified trousers-type test. By using the trousers-type fracture test the overall plastic bending kinematics of the fractured petal is preserved, as well as the mixed mode (mode one and mode three) fracture.

Through analytical and qualitative analysis, a testing apparatus to generate this trousers-type, plastic bending and mixed mode fracture was designed and machined.

Thesis Supervisor: Tomasz Wierzbicki
Title: Professor of Applied Mechanics

Thesis Reader: Jerome J. Connor
Title: Professor of Civil and Environmental Engineering

TABLE OF CONTENTS

LIST OF FIGURES

ACKNOWLEDGMENTS

I would like to thank Professor Wierzbicki and Professor Connor for their encouragement, enthusiasm, and guidance over the course of this project. I am indebted to their extensive knowledge and experience.

I would like to thank Steven Rudolph of the Department of Civil and Environmental Engineering Machine Shop for his extensive support and assistance in the design and fabrication of the equipment used in this study.

I would like to thank Hagbart S. Alsos for his generous assistance in creating preliminary numerical simulations for this study. His help prevented several potential shortfalls in the design and fabrication of the study equipment.

I would like to thank the U.S. Navy for providing me with the opportunity to study at M.I.T.

NOMENCLATURE

b	Rectangular tab width.
C	Parallel pre-cut length.
CTOA	Crack tip opening angle.
CTOD	Crack tip opening displacement.
F	Total instantaneous force exerted in one petal.
F_b	Wedge flap bending force.
F_f	Wedge cutting friction force.
F_m	Wedge cutting membrane force.
F_t	Total instantaneous force exerted in one rectangular tab.
F_W	Total minimum wedge cutting force.
F_{Wt}	Minimum instantaneous wedge cutting force.
G	Panel geometry parameter from Office of Naval Research (ONR) damage prediction model.
h	Plate thickness.
L_{AB}	Instantaneous length of petal hinge line.
M	Material properties parameter from ONR prediction model.
M_o	Fully plastic bending moment per unit length.
n	Number of symmetric petals in general petalling geometry.
R_h	Resultant hole size from ONR damage prediction model.
R_{min}	Minimum predicted hole size from ONR damage prediction model.
R_{max}	Maximum predicted hole size from ONR damage prediction model.
T	Plate thickness from ONR damage prediction model.
W_b	Bending work dissipated in one petal.
W_m	Membrane work dissipated in one petal.
W_t	Total work dissipated in one petal.
W_{TW}	Total minimum wedge cutting work.
x	Distance from instantaneous crack tip along crack/fracture.
x_p	Instantaneous length of plastic zone near crack tip.
γ	Angle of crack/fracture convergence.

δ	Instantaneous local crack width.
δ_{ctod}	Instantaneous crack tip opening distance.
δ_{mt}	Non-dimensional CTOD parameter.
δ_t	Crack tip opening displacement (CTOD) parameter.
Δ	Cross head vertical displacement.
Δ_{dot}	Cross head vertical speed.
η	Plastic bending moment amplification factor.
θ	Central petal semi-angle in general petalling geometry.
θ_{wedge}	Cutting wedge semi-angle.
λ	Instantaneous length of crack or fracture.
Λ	Instantaneous length of petal.
Λ_{dot}	Instantaneous petal length rate of change.
Λ_o	Pre-cut petal length.
ρ	Instantaneous radius of curvature of petal at the hinge line.
ρ_i	Rolling cylinder inner radius.
ρ_o	Rolling cylinder outer radius.
σ_o	Average flow stress.
ϕ	Instantaneous rotation of petal at hinge line.

INTRODUCTION

It is inherent in the design of any warship to provide robust resistance to hull and ship system damage under battle-type conditions. Since the extensive naval engagements of World War II there has been a sustained effort to study the detailed battle damage reports of naval vessels in the Pacific Theatre with the goal of understanding the mechanics of their damage and failure. This analysis led to the development of many protection systems, to abate the damage inflicted by gunfire, torpedo and mine attack. But as naval weapon technology rapidly developed in the post-World War II years, into the Cold War era and beyond, the damage mitigation systems have not kept pace. Little is known of the effects of modern naval weapons, such as anti-ship cruise missiles, advanced capability torpedoes, and shaped charge warheads, beyond the largely classified data provided by full-scale weapons tests on obsolete platforms. Even less is known about the battlefield efficacy of the modern systems designed to counter these new weapons.

The most recent data point for analysis is the damage of the U.S.S. COLE (DDG-67) on 12 October 2000 in the port of Aden Yemen. It is unofficially estimated that the state-of-the-art Arleigh Burke-class Guided Missile Destroyer was rocked by between 400 and 700 pounds of C-4 explosive detonated at the waterline, at a standoff of 0 to 10 feet from the hull. The extent of the damage to the ship can be clearly seen in Figure 1, showing the 20-foot by 40-foot hole torn into the port side hull of the ship.

As can be seen in this figure, a preponderance of the damage occurred below the waterline, and the overall characteristics of the damaged area were similar to the findings of Cole (1948, [24]), Wierzbicki, et al. (1996, [18] and 1999, [3]). The blast resulted in a spherical bulging, or dishing, of the hull plate prior to the onset of tearing, or petalling.

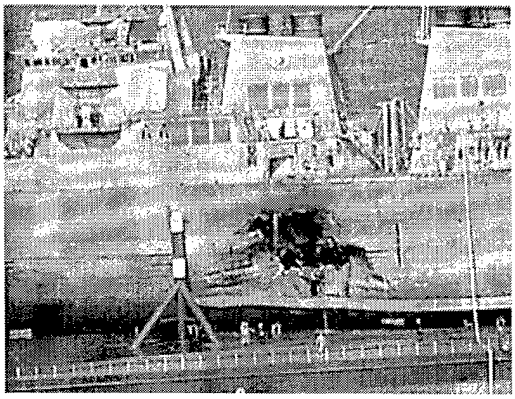

Figure 1: USS Cole Port Side Damage (from U.S. Navy Information Office)

The USS COLE was designed using the U.S. Navy survivability standards set forth in a series of Design Data Sheets (DDS's), specifically DDS 079-1 (1976) "Stability and Buoyancy of U.S. Navy Surface Ships," DDS 072-3 (1988) "Conventional Weapons Protection (fragments)," DDS 072-4 (1986) "Hull, Mechanical, and Electrical Systems Survivability," DDS 072-6 (1987) "Shaped Charge Warhead Weapon Effects Data," DDS 072-7 (1988) "Conventional Airblast (proximity)," and DDS 072-8 (1986) "Conventional Airblast (contact and internal) Design and Analysis Methodology." These design guidelines undertake to outline a systems-based approach to the mitigation of damage. They were conceived using classified explosive deformation and holing studies in naval vessels, empirically based on data accrued through years of live fire tests conducted by the Office of Naval Research (ONR).

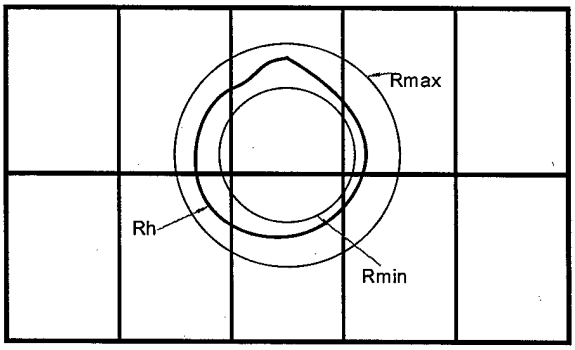

Figure 2: Current Stiffened Panel Damage Prediction Model

The resultant empirical engineering tool developed by ONR (Figure 2) suggests the general relationship:

$$R_{min} \leq R_h \leq R_{max} = f(G, T, M)$$

Where:

R_h = Resultant Hole Size

R_{min} = Minimum Predicted Hole Size

R_{max} = Maximum Predicted Hole Size

G = Panel Geometry

T = Plate Thickness

M = Material Properties

The direction of this study is to bring further illumination to the characteristics of T and M, Material Properties, in the above relationship. This research is primarily concerned with the cracking and petalling phase of fracture of hull plating subjected to a contact, underwater or air explosion. It will serve to augment previous work in relating blast-type failure of metal plate using a quasi-static approach. The objective is to provide a method to more easily obtain accurate data on the material properties of steel plate for this mode of failure.

STATEMENT OF PROBLEM

The investigation of holing failures in naval plate steel has been ongoing since the transition from wooden ships to steel, around the turn of the last century. The basis of most research in the field began with the goal of protecting naval ships from the penetration of artillery shells. Early research, conducted by Bertram Hopkins (1912), examined the resistance of various armor plating to ballistic particle penetration. His findings were among the first to illustrate the geometry of holing failure in metal plates, including plate dishing, and petalling from the formation of radial cracks, Figure 3.

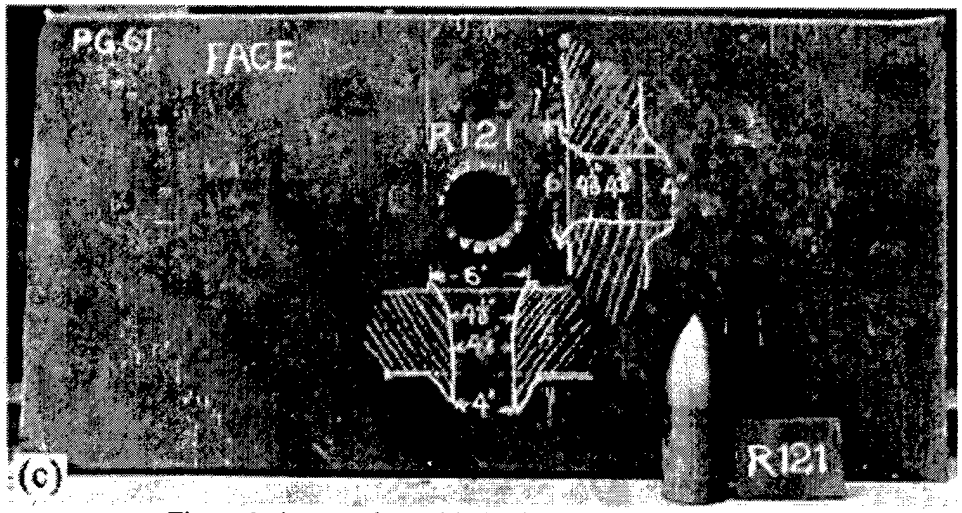

Figure 3: Armor Plate with Artillery Penetration (from Atkins et al. [15])

With the experiences of the two World Wars came concern for holing failure in naval ships from the explosive force of torpedo attack. Taylor (1948 [21]) and Cole (1948 [24]) conducted a comprehensive study of submerged blast waves and their effects on thin plates that formed the analytical basis of all current blast damage prediction methods. Although most subsequent research into this field, conducted by ONR, has been classified confidential, open-source study has been conducted on plate tearing and petalling caused by on-contact explosives by Keil (1956 [31] and 1961 [32]), Nurick (1996 [20]), Wierzbicki (1996 [18] and 1999 [3]), and Rajendran et al. (2001 [1]). The most comprehensive research

program in the perforation of plates by projectiles was conducted by Goldsmith et al. (1978 [38], 1983 [34], 1984 [35], 1984 [35], 1984 [36], 1984 [37]).

Through this not insubstantial body of data, the characteristics of mild and high strength steels have been extensively documented; however no simple, reliable method of predicting hull plate blast damage has been developed. Although computer codes for the prediction of blast damage are available, none provide more than a rough estimate of potential damage. As a result, nearly all of the definitive blast damage prediction is conducted using scaled, live fire tests, requiring substantial time and resources.

Within the last few decades there has been a drive to characterize and study the effects of these dynamic failure events using a quasi-static approach. This quasi-static approach to the issues of ballistic penetration and blast failure of metal plates has two purposes:

1. To relate the time-pressure history of the dynamic event to the corresponding force-displacement history of the quasi-static, and in so doing relate the incident blast wave energy directly to the plastic deformation and fracture in the material.

2. To work toward development of a fundamental crack propagation criterion through the examination of crack initiation and propagation and corresponding incremental strains.

These two purposes work toward the goal of improving existing computer finite element codes, leading to improved, simplified and reliable damage prediction tools.

To that end, research has been conducted relating the ballistic particle holing failure mode using a quasi-static method. Most recently, Atkins (1998 [15]) used conical and spherical penetrators to observe the necking, initial fracture (disking), and radial cracking (petalling) in ductile materials. Arndt et al. (2001 [16]) conducted further research illustrating the necking of thin sheets of aluminum around equibiaxially-expanded holes using a hydraulic bulger. Nazeer et al. (2000 [6]) using a conical tool, and Simonsen et al.

(2000 [5]) using a spherical indenter, analyzed the material mechanics of ductile metal sheets.

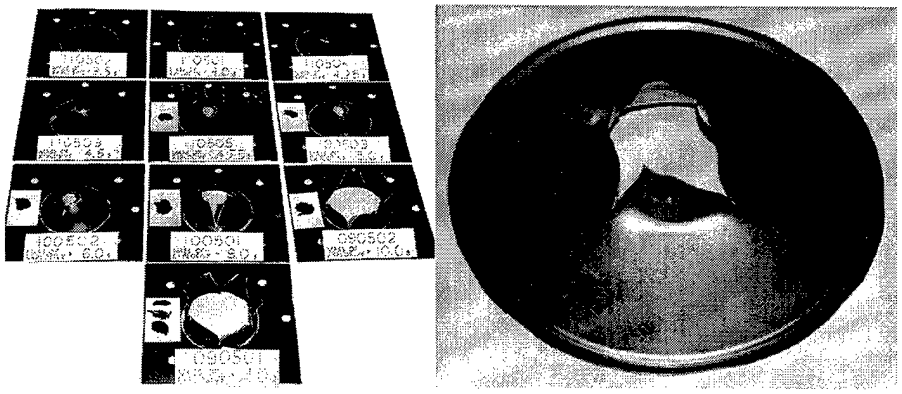

Figure 4: Dishing, Disking and Petalling of Plate under (L) Explosive Loading (from Wierzbicki [3]); (R) Lateral Indention by a Sphere (from Simonsen et al. [5])

Although these studies were primarily concerned with relating ballistic penetration using quasi-static methodology, they had a strong physical correlation with the behavior of thin sheets subjected to dynamic blast loading, see Figure 4. Additionally, after examining the plate cutting behavior of vessel groundings, Wierzbicki (et al. 1993 [7] and 1999 [3]) proposed that the kinematics of the thin plate cutting process, as seen in Figure 5, was comparable to those of both ballistic penetration and explosive petalling. To explore the extent of both of these physical correlations Woertz (2002 [4]) studied the deformation of clamped steel plates in two phases:

1. Using a spherical indenter to model early phase dishing, and subsequently disking.
2. Using an oblique conical punch to model late phase radial crack propagation and petalling.

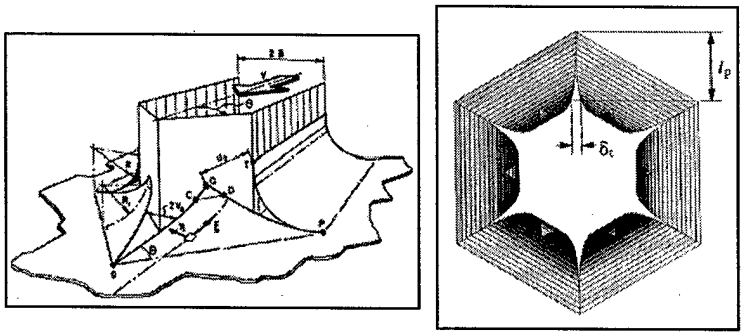

Figure 5: Similarity in the Kinematics of Wedge Cutting (Left) and Petalling (Right) (from Wierzbicki [3]).

This approach was largely successful in investigating the first phase, dishing and disking, but met some difficulty in the second. In addition to the physical limitations of the equipment used to induce radial cracking, Woertz also found the frictional interaction between the sample and the conical punch to be problematic in analyzing the force-displacement history.

The effects of friction in the wedge cutting model severely hamper its utility in the friction-free petalling phase of ballistic and blast failures. Woertz assumed only two components of work-energy dissipation in the petalling of thin metal sheets, bending work and membrane energy. Thomas (1992 [8]) estimated that in addition to bending and membrane work, friction accounts for as much as 40 percent of the work-energy dissipated in the mechanics of plate cutting. Zheng et al. (1996 [11]) characterized the frictional force on a wedge in the steady-state cutting of a plate as machining friction, near the tip, and sliding friction, along the sides of the wedge. Attempts by Lu et al. (1990 [10]) were made to quantify this frictional component in the cutting process by measuring the disengagement force of the cutting wedge. Yet no reliable method has been developed to accurately quantify the contribution of friction to the process of wedge cutting, and by extension quasi-statically model petalling and crack propagation.

An alternative approach to quasi-statically modeling crack propagation and petalling may be to use a variation of the trousers test of tearing ductile metal sheets. Yu et al. (1988 [17]) analyzed the energy dissipated in bending and tearing thin aluminum alloy sheets along

pre-machined grooves, using two counter-rotating cylinders, see Figure 6. This method preserved the key elements of petalling kinematics, including bending work and membrane energy, but removed the added effects of friction previously encountered, Figure 7. However, by pre-machining grooves, to guide the propagation of the tearing fracture, the material properties of the sample were altered, affecting the results. Lu et al. (1994 [33]) avoided this pre-machining by fashioning the sample of thin metal plate into a box column and allowing the tearing fracture to propagate along the corners. This approach also preserved the kinematics of petalling, but the geometric discontinuities of the sample at the sharp bends of the corners may have likewise affected the results.

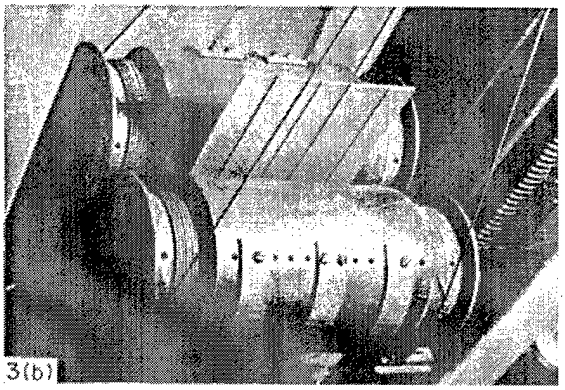

Figure 6: Counter-Rotating Cylinder Trousers Test
(from Yu et al. [17])

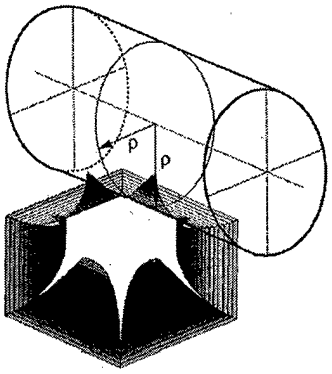

Figure 7: Cylindrical Roller Geometry of Petalling
(from Wierzbicki [3])

A possible solution to quasi-statically modeling the propagation of cracks and petalling of thin plates builds upon the work of Lu et al. Through the use of a similarly configured

testing apparatus and test samples, with specific connection tab details, a more accurate analysis of crack propagation and plate petalling may be made that incorporates plate bending energy, and membrane energy but avoids the inclusion of frictional, machining, and bending effects. This research develops a detailed apparatus design and method to conduct this analysis and compares testing results to analytically derived expected values.

TESTING METHOD AND APPARATUS DESIGN DEVELOPMENT

The development of the modified trousers test apparatus and method, for use as a quasi-static model for crack propagation and petalling was conducted in three phases. The first phase was an analytically based investigation of crack propagation and petalling with the purpose of defining gross load-displacement requirements of a detailed testing apparatus design. The second phase was a qualitative investigation of sample material preparation and test apparatus geometry in pursuit of an understanding of the characteristics, and possibly control of fracture propagation. The final phase was to develop a detailed testing apparatus design to be used in future studies to validate the quasi-static modeling method by testing samples of thin mild steel.

Analytical Investigation

Preliminary, order of magnitude, approximate analysis is included in the Analytical Investigation section of this paper, below.

Qualitative Investigation

Sample Preparation

The point of departure from previous trousers test studies of this work was the specific geometry of the sample. Previous trousers test samples used flat metal plates, with pre-cut, rectangular tabs, torn in the fashion of Figure 8. The purpose of these tests was to investigate the energy dissipation of tearing fractures, not in relation to cracking and petalling. Hence, the opposite, "reverse curvature" of every-other sample section was not of kinematic concern. However, to relate this type of tearing to crack propagation and petalling, including fracture and bending energy, it was important to isolate the curvature to a single portion of the sample material.

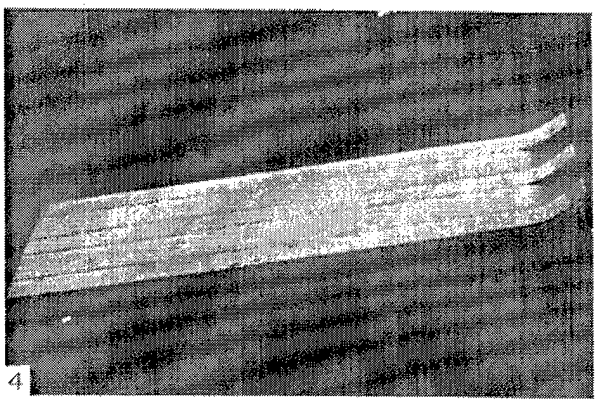

Figure 8: Trousers Test Sample with Pre-cut Rectangular Tabs and Machined Grooves(from Yu et al. [17]).

To achieve this type of tearing geometry, the thin sample plates were bent into box columns, in the fashion of the samples of Lu et al. However, while Lu attached the entire box edge to one of four cylindrical rollers, pre-cut tabs, located centrally on two opposing faces of the column edge attached the samples tested herein, Figure 9. This approach isolated the bending and curvature induced by the rollers to a flap of material out of the center of two opposing faces of the box, while maintaining an un-curved geometry for the remainder of the sample, better approximating the kinematics of petalling.

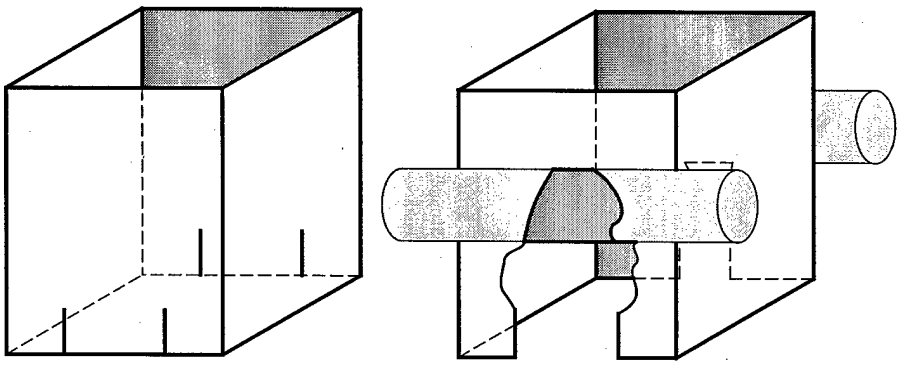

Figure 9: Rough Sample Geometry: (L) Pre-Cut Tabs Centrally Located on Opposing Faces, (R) Tabs Attached to Testing Apparatus.

In the tests of Yu et al. (1988 [17]) the propagation of the tearing fracture was controlled with the machining of grooves. In previous box column shaped samples the bent corners of the box column controlled the crack propagation, Lu et al. (1994 [33]).

With the samples of this study there was to be no machined or geometric preparations of the sample to govern the propagation of the tearing fracture. As a result, the first phase of this investigation was concerned with establishing the geometry of the connecting tabs on the box column sample, to best achieve data collection in the third phase. The aim of this first phase of testing was a qualitative understanding of the type of fracture propagation to expect during further phases of investigation, to see if the geometry of the connection tab influences the convergence or divergence of the fracture lines.

Apparatus Configuration

In further development of methods of controlling the propagation of fracture through the sample material, the effect of apparatus geometry to control the line of fracture propagation through the sample material was tested. Previous trousers tests used cylindrical metal rollers, with smooth and parallel surfaces, Figure 6. The purpose of this phase of testing was to investigate the effect of altering the shape of the surface of these cylindrical rollers and their position relative to the sample material to induce parallel lines of fracture propagation in the sample.

Apparatus Design

The final phase of this investigation consisted of utilizing the results of the previous two phases in the design of a modified trousers testing apparatus. This apparatus combines the analysis of the sample pre-cut and cylindrical roller geometry to govern the propagation of fractures through the sample material. This apparatus can then be used to conduct a series of modified trousers tests on thin mild steel plate (up to h=1mm) to model the petalling deformation caused by close proximity explosions, and comparing the detailed force-displacement data collected and computed specific work of fracture to analytical predictions.

ANALYTICAL INVESTIGATION

The general theory used in this section was first derived by Wierzbicki (1999 [3]) and simplified by Woertz (2002 [4]). They asserted that the total work dissipated in cracking and petalling is due to the propagation of the radial cracks, mechanical bending of the petals and membrane deformation. The bending analysis was developed from mechanical relations, and the membrane deformation derivation is an extension of the derivations of Wierzbicki et al. (1993 [7]). A full derivation of force-displacement relations is included in Appendix A.

General Petalling

Begin from very general petalling geometry of **n** cracks propagating from a single point, dividing a thin plate into **n** symmetric petals, Figure 10.

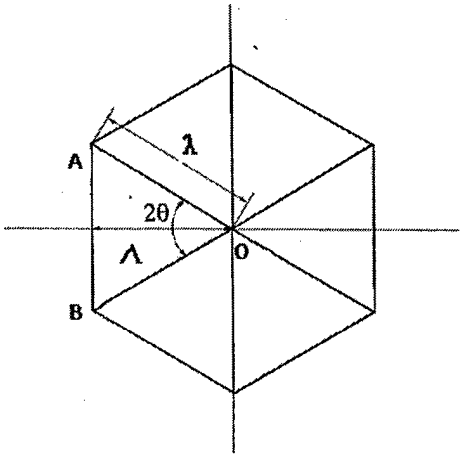

Figure 10: Theoretical Petalling Geometry

The central angle of each petal is defined as 2θ, such that:

$$\theta = \frac{\pi}{n} \tag{1}$$

And each petal can be described as a triangle **OAB**. The instantaneous length of the crack, λ, is related to the total petal length, Λ.

$$\lambda = \frac{\Lambda}{\cos(\theta)} \tag{2}$$

Bending Energy

As the petal grows in size, and the radial cracks propagate through the material, the hinge line **AB** moves through the material, leaving the curled petal behind. This kinematic boundary condition imposes a relation between the propagation speed of this hinge line, $d\Lambda/dt$, the instantaneous rate of rotation of the petal at the hinge line, $d\phi/dt$, and the instantaneous petal radius of curvature, ρ.

$$\frac{d}{dt}\phi = \frac{\frac{d}{dt}\Lambda}{\rho} \tag{3}$$

Wierzbicki ultimately derived an expression for ρ. In this study, the characteristics of the fixed cylinders of the testing apparatus dictate that the instantaneous radius of curvature of the petals is known and constant.

Continuing the assumption of a rigid, perfectly plastic material, with an average flow stress of σ_o, the fully plastic bending moment per unit length of the flat metal sheet, using the Tresca yield criteria, is:

$$M_o = \frac{\sigma_o \cdot h^2}{4} \tag{4}$$

where h is the plate thickness. Although Wierzbicki and Woertz continued to state that the curved, dished surface of the thin plate would stiffen, and amplify the plastic bending moment by the amplification factor η, the thin plate of this study remained flat and un-dished. Hence, $\eta=1$.

The rate of bending work of one petal is expressed as:

$$\frac{d}{dt}W_b = 2 \cdot M_o \cdot L_{AB} \cdot \frac{d}{dt}\phi \tag{5}$$

where $L_{AB}=2\Lambda\tan\theta$. Substituting Equation (3) into Equation (5) yields:

$$\frac{d}{dt}W_b = 4 \cdot M_o \cdot \Lambda \cdot \tan(\theta) \cdot \frac{\frac{d}{dt}\Lambda}{\rho} \tag{6}$$

To apply this to the quasi-static model of petalling used in this study, the changes in work dissipated over short increments of time and small increments of displacement can be obtained by integrating in time:

$$W = \int \frac{d}{dt} W \, dt \tag{7}$$

and Equation (6) becomes:

$$W_b = \frac{4 \cdot M_o \cdot \Lambda^2}{\rho} \cdot \tan(\theta) \tag{8}$$

Tearing Energy

For perfectly brittle materials, the crack width between adjacent petals can be expressed as a function of the distance from the point of intersection of two adjacent hinge lines.

$$\delta(x) = \frac{1}{3} \cdot \frac{x^3}{\rho^2} \cdot \sin(\theta) \cdot \cos(\theta)^3 \tag{9}$$

where δ is the local crack width, x is very near the crack tip, and ρ is constant. In real, ductile material, the crack tip does not coincide with the intersection of the hinge lines, but where local strain reaches the crack tip opening displacement parameter (CTOD) (Wierzbicki et al. 1993 [7]), δ_t. The length of the plastic zone near the crack tip can be found using CTOD and Equation (9):

$$x_p = 1.44 \rho^{\frac{2}{3}} \cdot \delta_t^{\frac{1}{3}} \cdot \sin(\theta)^{\frac{-1}{3}} \cdot \cos(\theta)^{-1} \tag{10}$$

Leading to the calculation of the rate of membrane energy dissipation in the plastic zone, near the crack tip:

$$\frac{d}{dt} W_m = \frac{\frac{2}{3} \cdot \sigma_o \cdot h \cdot x_p \cdot \frac{d}{dt} \Lambda}{\sin(\theta)} \tag{11}$$

Using Equations (4) and (10) in Equation (11):

$$\frac{d}{dt}W_m = \frac{3.84 M_o \cdot \delta_t^{\frac{1}{3}} \cdot \rho^{\frac{2}{3}} \cdot \sin(\theta)^{\frac{-4}{3}} \cdot \frac{d}{dt}\Lambda}{h \cdot \cos(\theta)} \tag{12}$$

To apply this to the same quasi-static model of petalling used in this study, the changes in work dissipated over short increments of time and small increments of displacement were again estimated, from Equation (7), and Equation (12) becomes:

$$W_m = \frac{3.84 M_o \cdot \delta_t^{\frac{1}{3}} \cdot \rho^{\frac{2}{3}} \cdot \Lambda \cdot \sin(\theta)^{\frac{-4}{3}}}{h \cdot \cos(\theta)} \tag{13}$$

Total Energy

Adding Equations (8) and (13) to get the total energy:

$$W_t = W_b + W_m \tag{14}$$

or:

$$W_t = \frac{4 \cdot M_o \cdot \Lambda^2 \cdot \tan(\theta)}{\rho} + \frac{3.84 M_o \cdot \Lambda \cdot \delta_t^{\frac{1}{3}} \cdot \rho^{\frac{2}{3}} \cdot \sin(\theta)^{\frac{-4}{3}}}{h \cdot \cos(\theta)} \tag{15}$$

To apply this to the quasi-static model of petalling used in this study, the changes in work dissipated over short increments of time and small increments of displacement were again estimated and Equation (15) becomes:

$$F = \frac{d}{d\Lambda}W_t \tag{16}$$

A force-displacement trace for this expression was generated for comparison between this analysis, and wedge cutting analysis, and is included in Appendix B. A general example of the generated force-displacement curves is computed in Appendix A, and included in Figure 11.

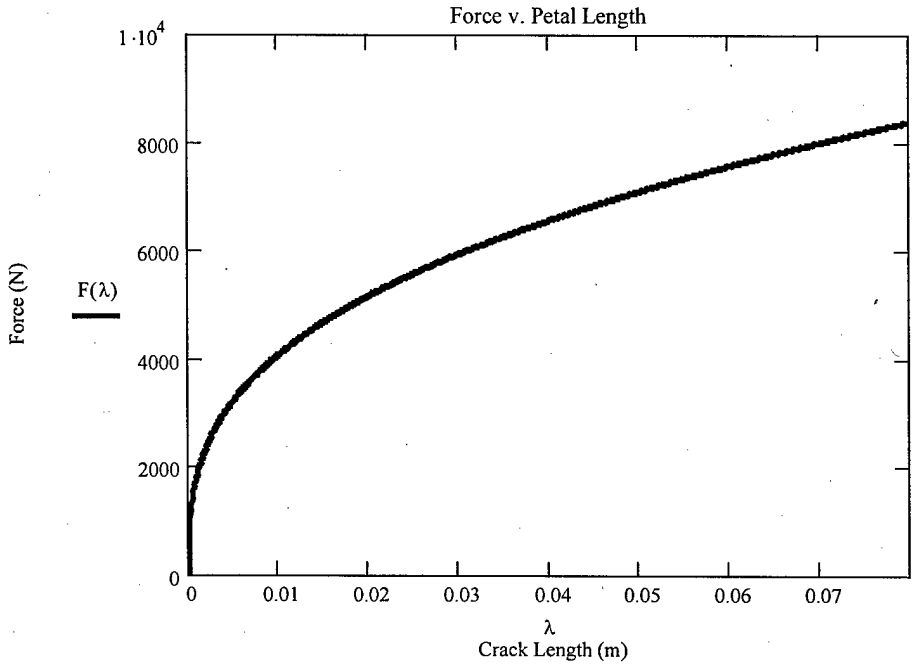

Figure 11: Approximate Theoretical Load-Displacement Curve for Petalled Plate

Expected Sample Energies

For the samples tested in this study, the geometry does not follow the general petalling geometry. Without the geometric or machined details of previous trousers tests the propagation of the fractures follows a path similar to those described in Simonsen et al. (1997 [12]) for the concertina tearing mode of plate failure. That is, the fracture propagation lines will not follow the angular petal lines, but will either become convergent or divergent, Figure 12.

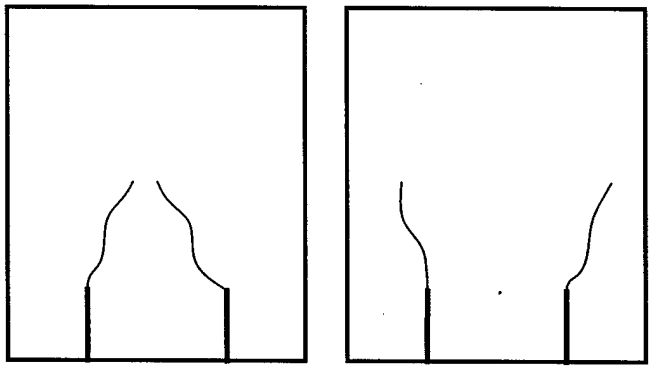

Figure 12: (L) Converging Fracture and (R) Diverging Fracture Geometries.

To that end, the sample and testing apparatus geometry were set to induce nearly parallel fractures. Hence, the general fracture geometry is no longer the triangular petals previously discussed, but becomes that of Figure 13.

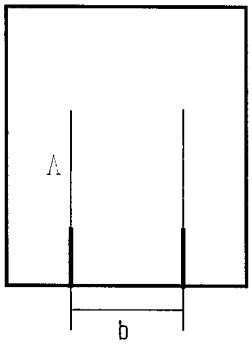

Figure 13: Sample Petalling Geometry

The lines of propagation of the non-ideal petal, or tab, are idealized as parallel and each petal can be described as a rectangular tab. The instantaneous length of the crack, λ, can be defined as a function of the total petal/tab length, Λ.

$$\lambda = \Lambda - C \tag{17}$$

Where C is the pre-cut length.

Bending Energy

Using the same assumption of a rigid, perfectly plastic material, with an average flow stress of σ_o, then the fully plastic bending moment per unit length of the flat metal sheet,

using the Tresca yield criteria, was previously derived, as Equation (4). The rate of bending work of one petal is expressed in Equation (5) with L_{AB}=b, or:

$$\frac{d}{dt}W_b = 2 \cdot M_o \cdot b \cdot \frac{d}{dt}\phi \tag{18}$$

Substituting Equation (3) into Equation (18) yields:

$$\frac{d}{dt}W_b = 2 \cdot M_o \cdot b \cdot \frac{\frac{d}{dt}\Lambda}{\rho} \tag{19}$$

To apply this to the quasi-static model of petalling used in this study, the changes in work dissipated over short increments of time and small increments of displacement can be obtained by integrating Equation (19) in time, to become:

$$W_b = \frac{2 \cdot M_o \cdot b \cdot \Lambda}{\rho} \tag{20}$$

Tearing Energy

Continuing the assumptions of the previous analysis, for perfectly brittle materials, the membrane energy rate of dissipation of on petal remains unchanged from Equation (12). The total membrane energy remains unchanged from Equation (13), with θ=60 degrees.

Total Energy

Adding Equations (20) and (13) to get the total energy:

$$W_t = \frac{2 \cdot M_o \cdot b\,\Lambda}{\rho} + \frac{3.84 M_o \cdot \Lambda \cdot \delta_t^{\frac{1}{3}} \cdot \rho^{\frac{2}{3}} \cdot \sin(\theta)^{\frac{-4}{3}}}{h \cdot \cos(\theta)} \tag{21}$$

To apply this to the quasi-static model of petalling used in this study, the changes in work dissipated over short increments of time and small increments of displacement were again calculated and Equation (21) becomes:

$$F_t = \frac{d}{d\Lambda}W_t \tag{22}$$

A general example of the generated force-displacement curves is computed in Appendix C, and included in Figure 14. Force-displacement curves corresponding to each sample tested are computed and included in Appendix H.

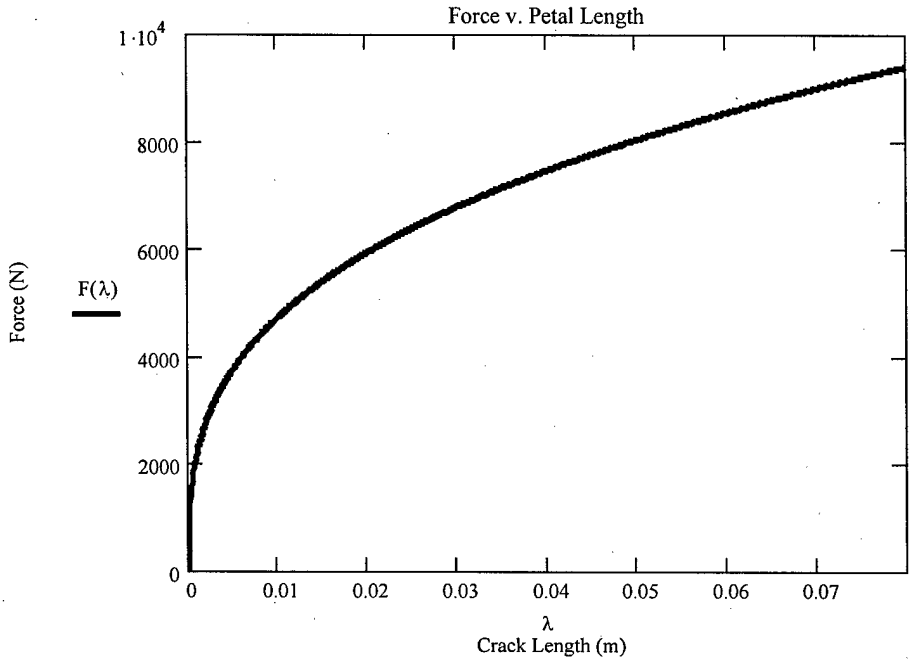

Figure 14: Approximate Theoretical Load-Displacement Curve for Tabbed/Petalled Sample Plate

QUALITATIVE INVESTIGATION

Sample Preparation

Method

To accomplish the second phase of this study, qualitative investigations of various tab geometries were carried out on thin gauge aluminum sheet, h=0.1117mm. Five tab geometries were fabricated onto the edges of flat samples, Figure 15, clamped on all four sides. The samples were subjected to tearing fractures using a rolling cylinder of radius ρ=1.5cm, and the behavior of the fracture propagation was noted and photographed, Appendix D.

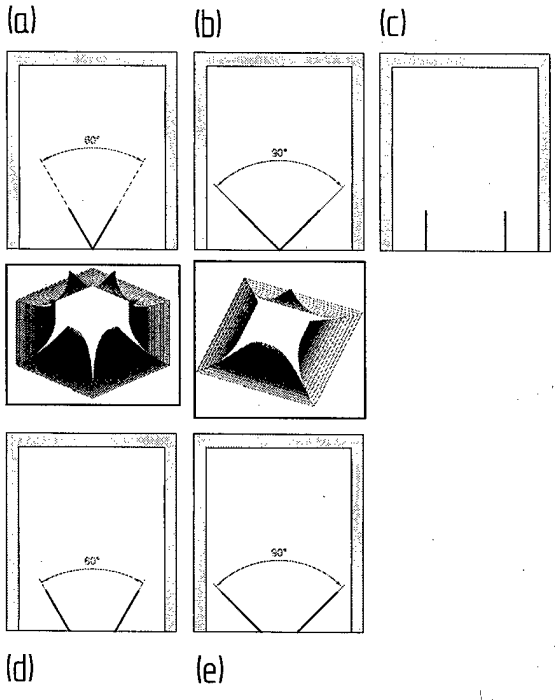

Figure 15: Qualitative Tab Sample Geometry (a) Six Petal Configuration, (b) Four Petal, (c) Trousers Configuration, (d) Six Petal Wide Tab Configuration, (e) Four Petal Wide Tab Configuration.

The first sample preparation was fabricated with pre-cut notches inclined at 60 degrees from the free edge, forming a 60-degree, triangular tab. This configuration was included to reproduce the geometry of a six-petal blast hole. The second sample was fabricated with

pre-cut notches inclined at 45 degrees from the free edge, forming a 90-degree, triangular tab. This configuration was to reproduce the geometry of a four-petal blast hole. The third sample configuration was fabricated with two parallel, pre-cut notches, forming a rectangular tab. This configuration was used for comparison to standard trousers test geometries. The fourth and fifth configurations were to reproduce the six and four petal geometry, respectively, with wider tabs to possibly accommodate fracture propagation.

Results

Figure 16 illustrates three cases of the fracture geometry encountered in the first phase of testing. The complete results of this testing phase are located in Appendix D. The sample geometries shown in the figure are the six petal pre-cut, the six petal wide tab, and the parallel pre-cut tab arrangement. From these representative cases it is seen that the cracks followed neither the line of the angled pre-cuts nor ran parallel through the aluminum sheet.

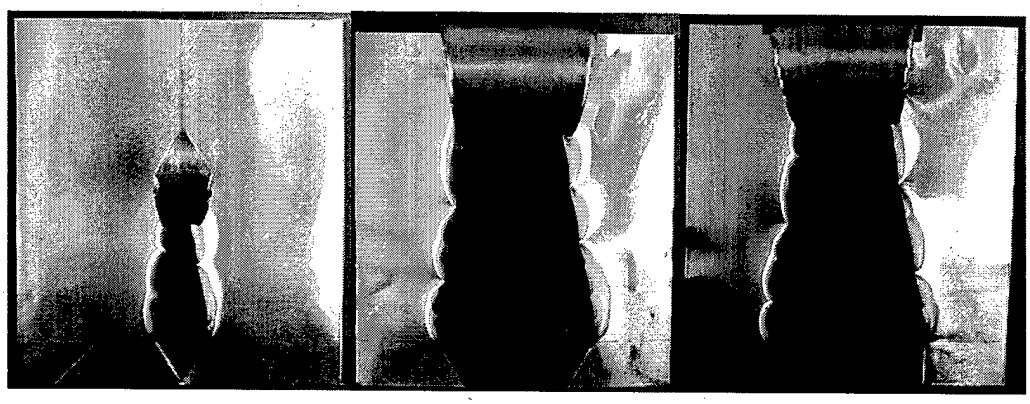

Figure 16: Phase One Results (L to R) n=6 Pre-cut Tab, n=6 Wide Pre-cut Tab and Parallel Pre-cut Tab.

As expected, all samples tested exhibited converging fracture lines, independent of pre-cut tab geometry. Further, the cracks of all samples converged at a relatively shallow angle, ranging from 7 to 10 degrees, and remained fairly straight. Complete results are found in Figure 17.

Figure 17: Comprehensive Phase One Results

Sample Number	Pre-Cut Geometry	Maximum Tab Width (mm)	Average Fracture Convergence Angle (deg)	Total Effective Fracture Length (mm)
1	90deg	30	6.8	80
2	90deg Wide	50	9.25	80
3	60deg	11.7	10.15	41
4	60deg Wide	50	7.8	80
5	Parallel	50	8.25	80

Discussion

From the results of this first phase of investigation it was seen that the line of propagation of the fractures induced by a rolling cylinder were independent of the pre-cut tab geometry. The angled pre-cuts experienced converging fracture lines of very similar convergence angles as the parallel pre-cuts. Further, all of the samples exhibited fairly constant convergence angles, resulting in straight fracture lines.

It was also observed in this phase of investigation that although the thin aluminum sheet was tightly clamped as the rolling cylinder progressed, the sample was stretched and became raised, or bowed, in the region of the rolled tab. It may be this bowing curvature and stretching of the material that induced the converging fracture geometry. It was this observation that provided motivation to conduct the second phase of investigation.

As a result of this first phase, it is asserted that the pre-cuts in the boxed material samples should be fabricated to ease connection of the sample to the testing apparatus, and maximize the overall fracture length. Both objectives may be achieved by widely spacing the pre-cuts on the face of the sample. The wider tab allows for a more secure connection between the sample material and the surface of the apparatus. The wider tab also allows for a longer fracture length before the fracture lines converge upon each other.

Additionally, the fairly constant angle of convergence encountered in this phase of testing suggests that analytical approximations of the force-displacement relations for each sample may be improved to account for this non-ideal fracture line geometry. The exact

convergence angle of each sample may be measured to impose this correction, or for very shallowly converging cracks the fracture line may be approximated as parallel for analysis.

Apparatus Configuration

Method

To accomplish the second phase of testing, qualitative investigations of various rolling cylinder geometries were carried out on thin gauge aluminum sheet, h=0.1117mm, with wide tab, 60 degree pre-cuts (Figure 15d). The samples were subjected to tearing fractures using three rolling cylinder face geometries, Figure 18, as in phase one of testing.

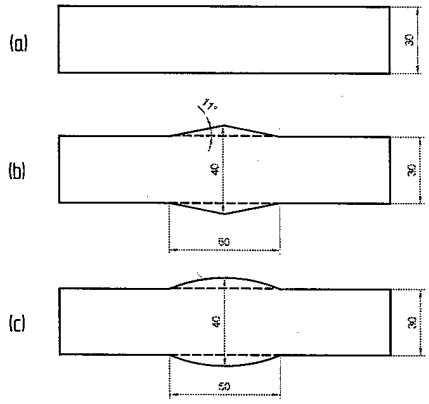

Figure 18: Qualitative Rolling Cylinder Geometry; (a) Parallel Cylinder, (b) Conically Tapered Cylinder, (c) Spherically Tapered Cylinder.

The first cylinder tested was a simple, parallel roller of ρ=15mm. This configuration was included to reproduce and compare the results encountered in the first phase of testing. The second cylinder was fabricated with a conically tapering radius, ρ_{max}=20mm. The third cylinder configuration was fabricated with a spherically tapering radius, ρ_{max}=20mm, ρ_{sphere}=65mm.

The two tapered cylinders were connected to the tabs of the thin aluminum in two configurations, Figure 19, flush to the point of maximum radius and recessed to the 15mm uniform radius.

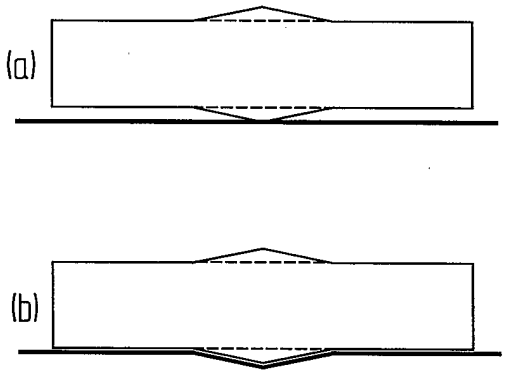

Figure 19: Phase Two Connection Geometry (a) Flush, (b) Recessed

The samples were subjected to tearing fractures using the three rolling cylinders, and the two connection geometries and the behavior of the fracture propagation was noted and photographed, Appendix F

Results

Figure 20 illustrates three cases of the fracture geometry encountered in the second phase of testing. The complete results of this testing phase are located in Appendix F. The sample geometry used in this phase, and shown in the figure, was the six petal pre-cut wide tab arrangement. The apparatus geometries illustrated in the figure are of the parallel and conically tapered cylinders, in the flush and recess mounted configurations. From these representative cases it is seen that the path of crack propagation was influenced by the geometry of the sample rolling apparatus.

Figure 20: Phase Two Results (L to R) Parallel Face Cylinder, Flush Mounted Conically Tapered Cylinder and Recess Mounted Conically Tapered Cylinder.

As seen in the complete Phase Two data, the geometry of the cylinder face alone did not have a profound effect upon the convergence of the fracture lines through the thin aluminum sample. That is, the flush mounted conically tapered cylinder had fracture lines converging at a rate not dissimilar to those of spherically tapered cylinder and the parallel, simple cylinder. Of greater effect upon the fracture propagation was the detail of connection between the sample and the roller. Specifically, recessing the conically or spherically tapering segment of the cylinder significantly reduced the angle of convergence of the fracture lines in the samples. Complete results are found in Figure 21.

Figure 21: Comprehensive Phase Two Results

Sample Number	Cylinder Geometry	Connection Geometry	Average Fracture Convergence Angle (deg)
1	Parallel	Flush Mounted	7.8
2	Conically Tapering	Flush Mounted	5.65
3	Spherically Tapering	Flush Mounted	4.55
4	Conically Tapering	Recessed	2.1
5	Spherically Tapering	Recessed	2.5

Discussion

From the results of this second phase of investigation it was seen that the line of propagation of the fractures induced by a rolling cylinder were influenced by the geometry of the face of the cylinder. Cylinders with regions of convex tapered radii induced shallower angles of fracture convergence than simple, parallel-faced cylinders. Further, it was found that the method of connection between the thin aluminum sample and the convex tapered cylinder also influenced the angle of convergence. By recessing the region of convexity into the sample, the result of connecting the sample material to the non-convex parallel region of the cylindrical roller, the fracture lines could be made nearly parallel.

As a result, it is asserted that the propagation of the fracture lines through the sample material in the third phase of this investigation may be controlled using methods other than physically altering the sample. Through the addition of a convex region to the face of the rolling cylinders, and the recessed attachment of the sample material to the cylinders, nearly parallel fracture lines can be induced.

APPARATUS DESIGN

Using the results of the second phase of testing, box column samples as seen in Figure 22 are to be constructed for use on the test apparatus. Complete test sample specifications are included in Appendix E. The samples are to be inserted into the testing apparatus as illustrated in Figure 23. Complete testing apparatus specifications are included in Appendix G. The two rollers are then to be driven simultaneously by pulling up the four attached wire ropes. This motion causes bending of the two pre-cut tabs onto the rollers, and at the same time propagates tearing along the two opposite sample faces.

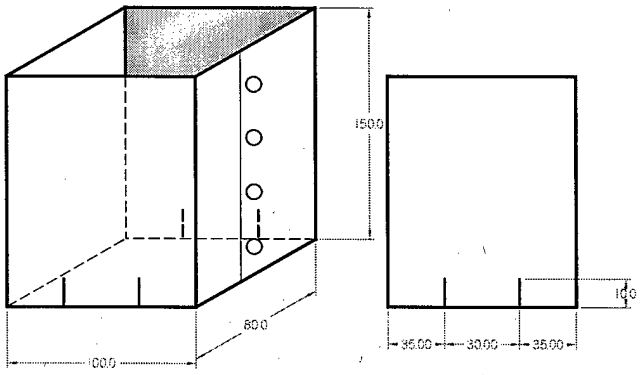

Figure 22: Box Column Sample Geometry

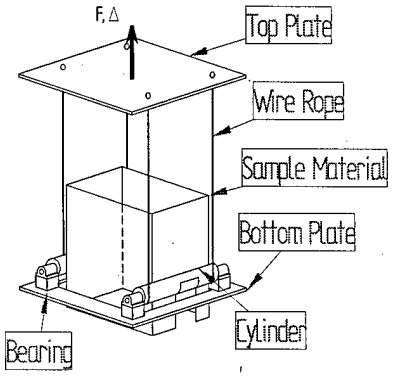

Figure 23: Schematic of Experimental Setup

CONCLUSIONS AND RECOMMENDATIONS

Conclusions:

Through the preliminary theoretical analysis it was found that comparison between wedge cutting and petalling kinematics, based on similar geometry, is well grounded. As seen in Appendix B, force displacement relationships in each case are nearly identical when the effect of wedge cutting friction is neglected. However, in actual wedge cutting processes, the effect of friction is great, and negates the utility of comparison between the two phenomena.

As a superior method of recreating the same petalling process using a quasi-static approach, the modified trousers test of this study proved useful. It was initially found that petalling-like fractures in thin metal samples could be reliably produced using a rolling cylinder, which generated converging lines of fracture. This convergence was postulated to be the result of the ductile characteristics of the thin samples giving rise to mixed mode, in-plane and out-of-plane, tearing. Hence, analyzing force-displacement data using an idealized, triangular petal was revealed to be inadequate. The plastic hinge line, propagating away from the tip of the petal, decreases in length in a converging geometry, as opposed to expanding in length in the idealized model.

It proved more accurate to model the petalling fracture propagation as a rectangular tab, with parallel lines of fracture. This compelled the development of a method to offset the convergence of fracture lines, and produce parallel fractures. This was to be achieved without altering the sample geometry or material properties, as inadvertently done in past trousers tests (Lu et al. 1994 [33] and Yu et al. 1988 [17]). It was shown that altering the geometry of the sample pre-cuts had little effect on the lines of fracture through the sample. Better results were achieved in controlling the fracture convergence by changing the shape of the cylindrical roller. Through the addition of a raised portion to the cylinder face, the angles of convergence in the sample were modestly reduced. Altering the connection geometry of the raised portion of the cylinder to the sample material proved most successful in controlling the angle of fracture convergence. Through the combination

of the raised cylinder face and modified connection detail, the lines of fracture were made nearly parallel.

With this knowledge, the modified trousers testing apparatus was constructed, as detailed in Appendix G, and sample specimens were fabricated, as detailed in Appendix E.

Recommendations

Most necessary in future work is an extensive study using the newly constructed testing apparatus and modified trousers test method to thoroughly validate this quasi-static approximation of the fracture and petalling phenomena. Further investigations should include a range of sample thickness, up to a maximum thickness of 1mm (for mild steel). Additionally, through testing multiple materials a greater understanding of the petalling process could be achieved.

In future studies using the modified trousers test apparatus an analysis of the strain field, near the crack tip should be conducted. In a method similar to that used by Woertz (2002 [4]), fine grid markings could be made on the sample faces to compute instantaneous local strains. These strains could be used as a measure of material stretching, three dimensional petal displacements, and bending work dissipated in achieving the final deformed geometry. From such an analysis, a more defined understanding of total work dissipated could be achieved, aiding in an understanding of the methods of energy dissipation in the initial phase of dynamic, explosive events.

In conjunction with an investigation of the strain field, perhaps a superior method of computing the displacement of the sample material could be developed. In stead of wholly relying on the position of the testing machine cross-head, and from there calculating the relative motion of the sample, to determine strain, measuring displacements directly from the sample may prove more useful for the analysis of the crack tip strain field. Measuring sample displacements directly could be effected indirectly, by measuring the angle of rotation of each roller, or directly, by measuring a pre-determined point on the sample to a fixed point in space.

Perhaps most significantly, results from future tests using the modified trousers test apparatus should be compared to results obtained from existing numerical models. Such models could be constructed in ABAQUS or LS-DYNA to investigate the mode and location of fracture, and approximate the deformed sample shape as the result of fracture. Further, such numerical results would serve to improve upon the design of the apparatus. Specifically, through an understanding of the details of fracture the shape of the cylindrical rollers could be improved to further control fracture convergence.

BIBLIOGRAPHY

[1] Rajendran, R. and K. Narasimhan (2001), "Damage prediction of clamped circular plates subjected to contact underwater explosion," International Journal of Impact Engineering, Vol. 25, pp 373-386.

[2] Jones, N. and C. Jones (2002), "Inelastic failure of fully clamped beams and circular plates under impact loading," Journal of Mechanical Engineering Science, Vol. 216, Part C, pp133-149.

[3] Wierzbicki, T. (1999), "Petalling of plates under explosive and impact loading," International Journal of Impact Engineering, Vol. 22, pp935-954.

[4] Woertz, J. (2002), "Quasi-static tearing tests of metal plating," M. Sc. Thesis, Massachusetts Institute of Technology.

[5] Simonsen, Bo Cerup and Lars Peder Lauridsen (2000), "Energy absorption and ductile failure in metal sheets under lateral indention by a sphere," International Journal of Impact Engineering, Vol. 24, pp1017-1039.

[6] Nazeer, Malik M., M. Afzal Khan, Anther Naeem, and Anwar-ul Haq (2000), "Analysis of conical tool perforation of ductile metal sheets," International Journal of Mechanical Sciences, Vol. 42, pp1391-1403.

[7] Wierzbicki, T. and P. Thomas (1993), "Closed-form solution for wedge cutting force through thin metal sheets," International Journal of Mechanical Sciences, Vol. 35, No. 3/4, pp209-229.

[8] Thomas, Paul (1992), "The mechanics of plate cutting with application to ship grounding," M. Sc. Thesis, Massachusetts Institute of Technology.

[9] Jones, N. and W.S. Jouri (1987), "A study of plate tearing for ship collision and grounding damage," Journal of Ship Research, Vol. 31, No. 4, pp253-268.

[10] Lu, G. and C.R. Calladine (1990), "On the cutting of a plate by a wedge," International Journal of Mechanical Science, Vol. 32, No. 4, pp293-313.

[11] Zheng, Z.M. and T. Wierzbicki (1996), "A theoretical study of steady-state wedge cutting through metal plates," International Journal of Fracture, Vol. 78, pp45-66.

[12] Simonsen, Bo Cerup and T. Wierzbicki (1997), "Plasticity, fracture and friction in steady-state plate cutting," International Journal of Impact Engineering, Vol. 19, No. 8, pp667-691.

[13] Bracco, M. (1994), "A study on the wedge cutting force through longitudinally stiffened plates: an application to grounding resistance of single and double hull ships," M. Sc. Thesis, Massachusetts Institute of Technology.

[14] Paik, Jeom (1994), "Cutting of a longitudinally stiffened plate by a wedge," Journal of Ship Research, Vol. 38, No. 4, pp340-348.

[15] Atins, A.G., M. Afzal Kahn and J.H. Liu (1988), "Necking and radial cracking around perforations in thin sheets at normal incidence," International Journal of Impact Engineering, Vol. 21, No. 7, pp521-539.

[16] Arndt, S., S. Swillo, and A.G. Atkins (2001), "Multiple necks around biaxially loaded holes in sheets," International Journal of Mechanical Sciences, Vol. 43, pp245-263.

[17] Yu, T.X., D.J. Zhang, Y. Zhang and Q. Zhou (1988), "A study of the quasi-static tearing of tin metal sheets," International Journal of Mechanical Science, Vol. 30, No. 3/4, pp193-202.

[18] Wierzbicki, T. and G.N. Nurick (1996), "Large deformation of thin plates under localized impulsive loading," Engineering Fracture Mechanics, Vol. 20, No. 1, pp159-167.

[19] Nurick, G.N. and G.C. Shave (1996), "The deformation and tearing of thin square plates subjected to impulsive loads – An experimental study," Engineering Fracture Mechanics, Vol. 18, No. 1, pp99-116.

[20] Nurick, G.N., M.E. Gelman and N.S. Marshall (1996), "Tearing of blast loaded plates with clamped boundary conditions," Engineering Fracture Mechanics, Vol. 18, No. 7, pp803-827.

[21] Taylor, G.I. (1948), "The formation and enlargement of a circular hole in a thin plastic sheet," Quarterly Journal of Mechanics and Applied Mathematics, Vol. 1, pp103-124.

[22] McClintock, F.A. and Z.M. Zheng (1993), "Ductile fracture before localized necking in a strip under tension," International Journal of Fracture, Vol. 64, pp191-200.

[23] Taylor, G.I. (1948), The pressure and impulse of submarine explosion waves on plates," The Scientific Papers of Sir Geoffrey Ingram Taylor, Vol. 3, No. 31, pp287-303.

[24] Cole, R.H. (1948), Underwater Explosions, Princeton University Press.

[25] Shames, I.H. (1989), Introduction to Solid Mechanics, Prentice-Hall.

[26] Huges, O. (1988), Ship Structural Design, The Society of Naval Architects and Marine Engineers.

[27] Riley, W.F. and L. Zachary (1989), Introduction to Mechanics of Materials, John Wiley and Sons.

[28] Tedesco, J., W. McDougal and C.A. Ross (1999), Structural Dynamics Theory and Application, Addison Wesley Longman.

[29] Design Data Sheet 079-1, "Stability and buoyancy of U.S. Naval surface ships," Department of the Navy, Naval Ship Engineering Center.

[30] Design Data Sheet 072-4, "Hull, Mechanical and Electrical Systems, Survivability," Department of the Navy, Naval Ship Engineering Center.

[31] Keil, A.H. (1956), "The response of ships to underwater explosions," Transactions of the Society of Naval Architects and Marine Engineers, Vol. 69, pp366-410.

[32] Keil, A.H. (1961), Introduction to underwater explosion research, UERD, Norfolk Naval Shipyard, Portsmouth, Virginia.

[33] Lu, G., L.S. Ong, B. Wang, H.W. Ng (1994), "An experimental study on tearing energy in splitting square metal tubes," International Journal of Mechanical Sciences, Vol. 36, pp1087-1097.

[34] Goldsmith, W., J. Liss, J.M. Kelly (1983), "A phenomenological penetration model of plates," International Journal of Impact Engineering, Vol. 1, No. 4, pp321-342.

[35] Liss, J., W. Goldsmith (1984), "Plate perforation phenomena due to normal impact by blunt cylinders," International Journal of Impact Engineering, Vol. 2, No. 1, pp37-64.

[36] Levy, N., W. Goldsmith (1984), "Normal impact and perforation of thin plates by hemisphercally-tipped projectiles – I Analytical considerations," International Journal of Impact Engineering, Vol. 2, No. 3, pp209-230.

[37] Levy, N., W. Goldsmith (1984), "Normal impact and perforation of thin plates by hemisphercally-tipped projectiles – II Experimental results," International Journal of Impact Engineering, Vol. 2, No. 4, pp299-324.

[38] Backman, M.E., W. Goldsmith (1978), "The mechanics of penetration of projectiles into targets," International Journal of Engineering Sciences, Vol. 16, pp1-99.

APPENDIX A: PETALLING FORCE-DISPLACEMENT APPROXIMATION

For a sample plate of thin, ductile metal with the following characteristics:

$h := .5 \cdot mm$ — Plate thickness

$\sigma_o := 272 \cdot 10^6 \cdot Pa$ — Average Flow Stress

$CTOA := 10 \cdot deg$ — Crack tip opening angle (CTOA)

And petalling geometry:

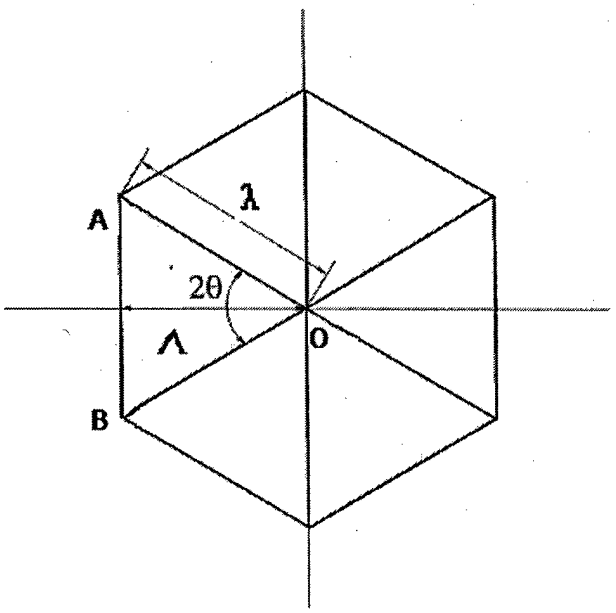

$\theta := 30 \cdot deg$ — Corresponding to petal semi-angle

where n=6

$\Lambda_o := 1.5 \cdot cm$ — Pre-cut petal length

On the testing apparatus with the following characteristics:

$\rho_o := 1.5 \cdot cm$ — Rolling cylinder radius

$$\rho_i := 1.25 \cdot cm$$

Wire rope cylinder radius

$$\Delta_{dot} := 10 \cdot \frac{mm}{min}$$

Cross-Head vertical speed

$$\Lambda(\lambda) := \lambda \cdot \cos(\theta) + \Lambda_c$$

Total petal length as a function of fracture length

$$\lambda(\Delta) := \Delta \cdot \frac{\rho_o}{\rho_{wr}} \cdot \cos(\theta)^{-1}$$

Fracture length as a function of cross-head vertical displacement

Resulting in:

$$\Lambda_{dot} := \Delta_{dot} \cdot \frac{\rho_o}{\rho_i}$$

Petal length rate of change

$$\delta_{ctod}(\lambda) := 2 \cdot \lambda \cdot \sin(CTOA)$$

Crack tip opening distance as a function of fracture length

$$\delta_{ctod}(\Delta) := 2 \cdot \Delta \cdot \frac{\rho_o}{\rho_{wr}} \cdot \cos(\theta)^{-1} \sin(CTOA)$$

CTOD as a function of cross-head displacement

Total bending moment per petal per unit length

$$M_o := \frac{\sigma_o \cdot h^2}{4}$$

$$M_o = 17 \frac{N \cdot m}{m}$$

$$W_b(\lambda) := \frac{4 \cdot M_o \cdot (\Lambda(\lambda) - \Lambda_o)^2 \cdot \tan(\theta)}{\rho_o}$$

Total bending work per petal as a function of fracture length

$$W_b(\Delta) := \frac{4 \cdot M_o \cdot \left(\Delta \cdot \frac{\rho_o}{\rho_{wr}}\right)^2 \cdot \tan(\theta)}{\rho_o}$$

Total bending work per petal as a function of cross-head displacement

And the contribution of membrane work was expressed as:

$$W_m(\lambda) := M_o \cdot (\Lambda(\lambda) - \Lambda_o) \cdot 3.84 h^{-1} \cdot (\delta_{ctod}(\lambda))^{\frac{1}{3}} \cdot (\rho_o)^{\frac{2}{3}} \cdot \sin(\theta)^{\frac{-4}{3}} \cdot \cos(\theta)^{-1}$$

or:

$$W_m(\Delta) := M_o \cdot \left(\Delta \cdot \frac{\rho_o}{\rho_{wr}}\right) \cdot 3.84 h^{-1} \cdot (\delta_{ctod}(\Delta))^{\frac{1}{3}} \cdot (\rho_o)^{\frac{2}{3}} \cdot \sin(\theta)^{\frac{-4}{3}} \cdot \cos(\theta)^{-1}$$

Making the total work:

$$W_t(\Delta) := W_m(\Delta) + W_b(\Delta)$$

And the total force:

$$F(\Delta) := \frac{d}{d\Delta} W_t(\Delta)$$

Traces of force and work as a function of crack length:

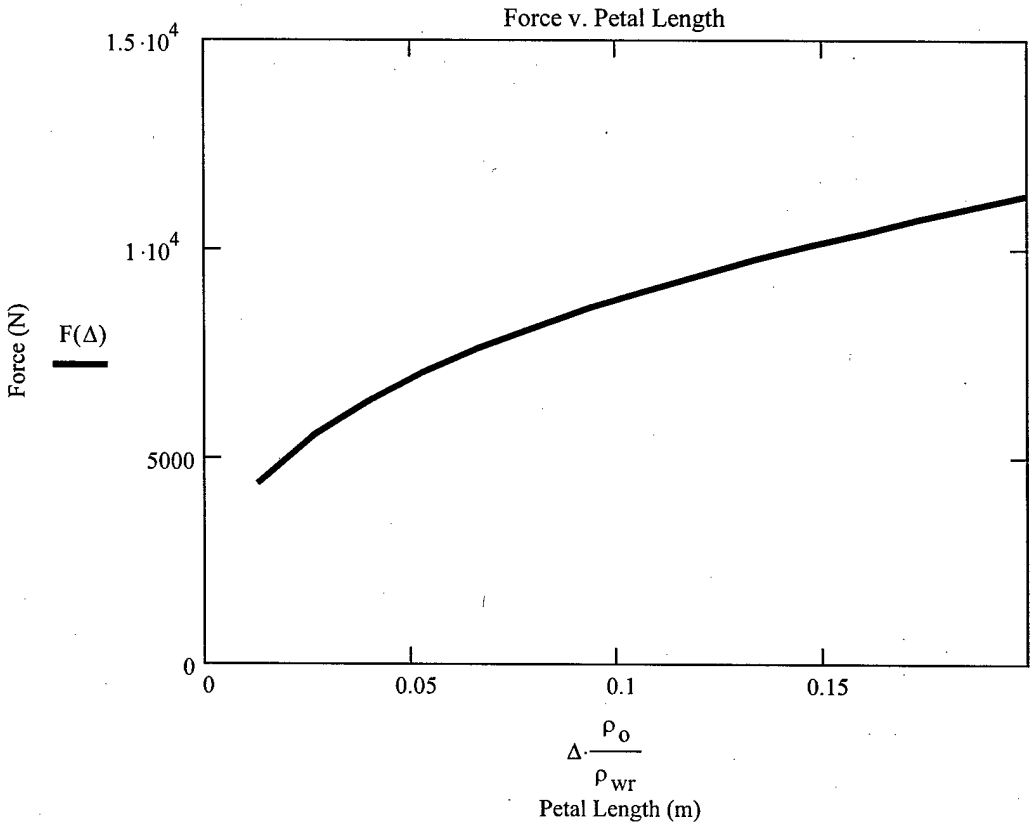

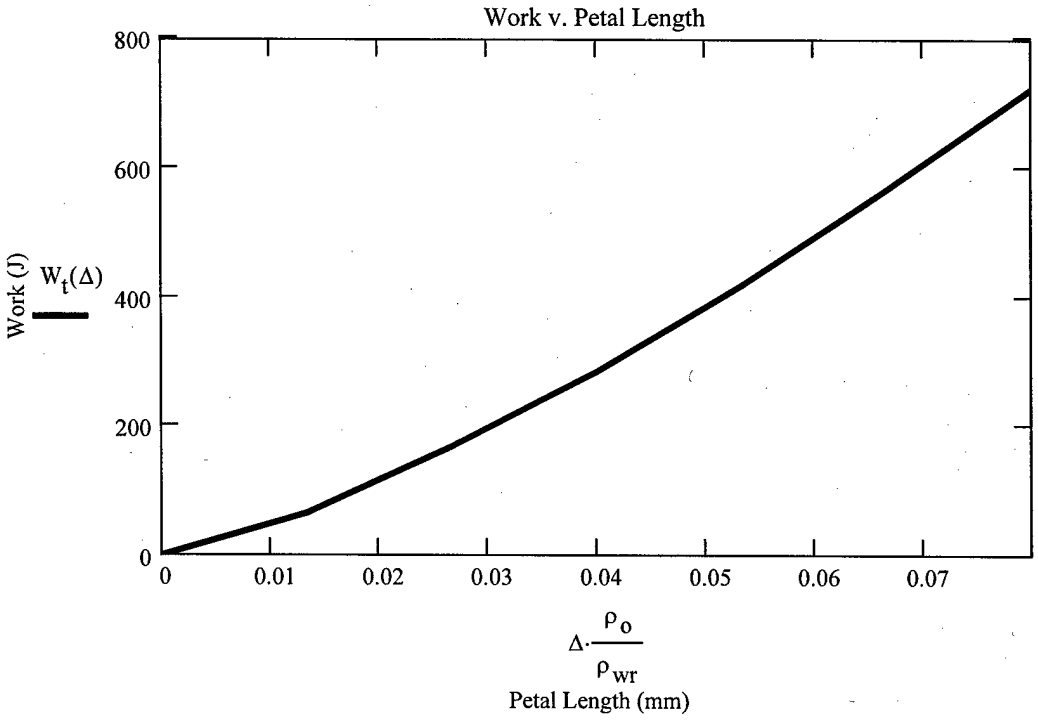
Work v. Petal Length
800
600
400
200
0
Work (J)
$W_t(\Delta)$
0
0.01
0.02
0.03
0.04
0.05
0.06
0.07
$\Delta \cdot \frac{\rho_o}{\rho_{wr}}$
Petal Length (mm)

APPENDIX B: PETALLING AND WEDGE CUTTING

For a sample plate of thin, ductile metal with the following characteristics:

$h := .5 \cdot mm$ — Plate thickness

$\sigma_o := 272 \cdot 10^6 \cdot Pa$ — Average Flow Stress

$CTOA := 10 \cdot deg$ — Crack tip opening angle (CTOA)

And petalling geometry:

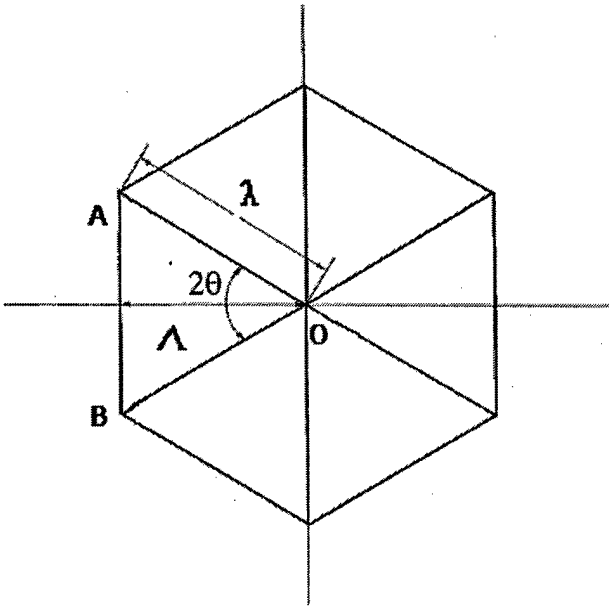

$\theta := 30 \cdot deg$ — Corresponding to petal semi-angle where n=6

$\Lambda(\lambda) := \lambda \cdot \cos(\theta)$ — Petal length as a function of crack length

Woertz (2002 [4]) built upon the derivations of Wierzbicki (1999 [3]) to derive simplified expressions for the total work dissipated in the formation of radial cracks and petals. For application to the testing of this work, the instantaneous radius of curvature of

the petals was made constant, to reflect the curvature induced by the cylinders of the testing apparatus:

$\rho_o := 1.5 \cdot cm$ Rolling cylinder radius

Other characteristics of the testing apparatus:

$\Delta_{dot} := 10 \cdot \frac{mm}{min}$ Cross head speed

$\Delta(\lambda) := \Lambda(\lambda)$ Cross head vertical displacement

Woertz also decomposed the total work into contributions of bending work and membrane work. As that petalling is a frictionless process, he included no contribution of friction in his simplified expressions. The bending work was expressed as:

$M_o := \frac{\sigma_o \cdot h^2}{4}$ $M_o = 17 \frac{N \cdot m}{m}$

Total bending moment per petal per unit length

$W_b(\lambda) := \frac{4 \cdot M_o \cdot (\Lambda(\lambda))^2 \cdot \tan(\theta)}{\rho_o}$ Total bending work per petal

And the contribution of membrane work was expressed as:

$\delta_{ctod}(\lambda) := 2 \cdot \lambda \cdot \sin(CTOA)$ Crack tip opening distance

$W_m(\lambda) := M_o \cdot \Lambda(\lambda) \cdot 3.84 h^{-1} \cdot (\delta_{ctod}(\lambda))^{\frac{1}{3}} \cdot (\rho_o)^{\frac{2}{3}} \cdot \sin(\theta)^{\frac{-4}{3}} \cdot \cos(\theta)^{-1}$

Making the total work:

$W_t(\lambda) := W_m(\lambda) + W_b(\lambda)$

And the total force:

$F(\lambda) := \frac{d}{d\Delta} W_t(\lambda)$

For a petal length of 70mm the force and work are:

$F(70 \cdot mm) = 8.004 \times 10^3\ N$ $\qquad$ $W_t(70 \cdot mm) = 415.384 J$

And traces of force and work as a function of crack length:

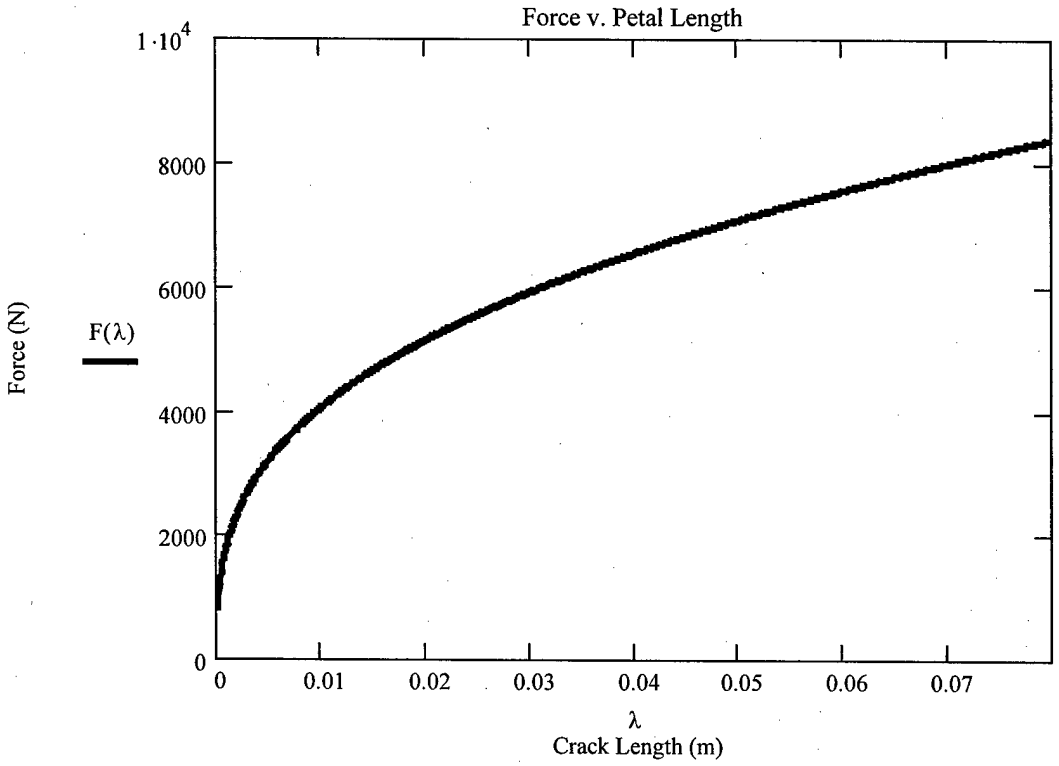

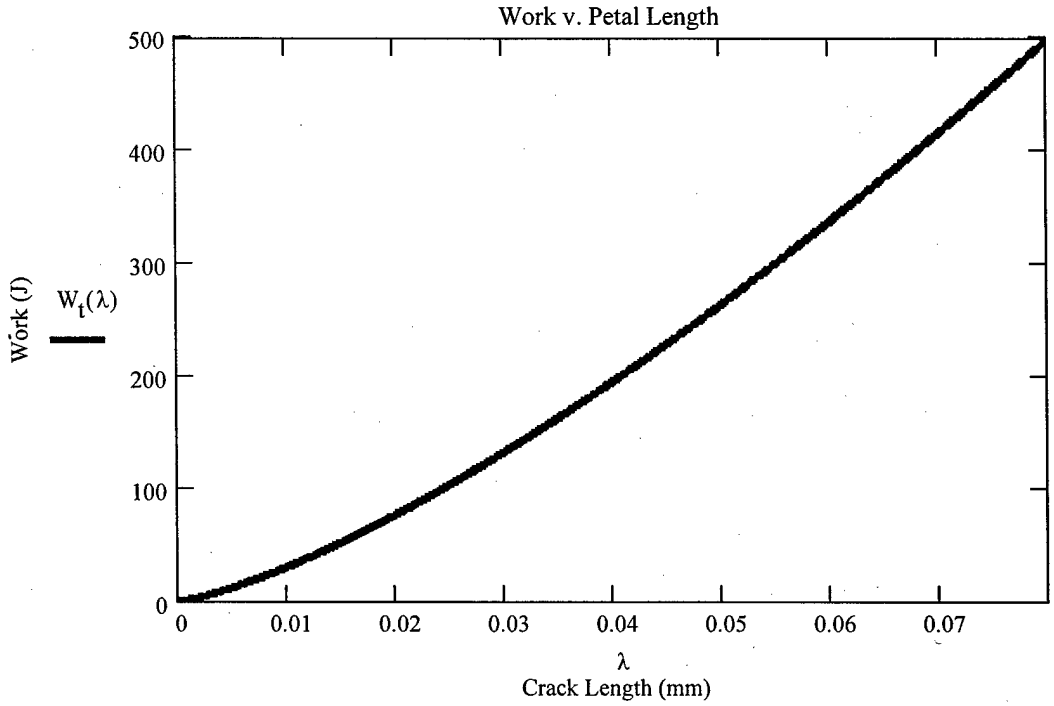

For analytic comparison, Wierzbicki & Thomas (1993 [7]) derive expressions to produce the minimum cutting force of a wedge through a thin plate with the following characteristics:

$$\delta_{mt}(\lambda) := \frac{\delta_{ctod}(\lambda)}{h}$$

Non-dimensional CTOD parameter

$$\theta_{wedge} := 60 \cdot deg$$

Wedge semi-angle equal to the petalling angle, corresponding to n=6

As the sum of three components:

$$F_w = F_b + F_m + F_f$$

Where:

F_w = Minimum Cutting Force for One Fracture

F_b = Flap Bending Force for One Fracture

F_m = Membrane Force for One Fracture

F_f = Friction Force for One Fracture

The underlying assertion of Wierzbicki & Thomas is that, with the elimination of wedge friction, accounted for in their derivation but difficult to experimentally measure, the wedge cutting model can be successfully applied to the petalling and cracking model. Hence, for purposes of comparison to Woertz, the frictional component of the crack propagation is ignored, and the expression derived is:

$$F_w(\lambda) := 1.67 \cdot \sigma_o \cdot \delta_{mt}(\lambda)^{.2} \cdot h^{1.6} \cdot \lambda^{.4} \cdot \sin(\theta_{wedge})^{.4} \cdot \cos(\theta_{wedge})^{-1.2}$$

Leading to the derivation of the work dissipated in one fracture as a function of fracture length:

$$W_{tw}(\lambda) := \int_0^{\lambda} F_w(\phi)\, d\phi$$

To apply these expressions for use in crack propagation and petalling, it is most important to notice that each petal consists of two of these wedge-like fractures. Hence:

$F_{WT}(\lambda) := 2 \cdot F_w(\lambda)$ Total Petalling Force (Wierzbicki & Thomas) as a function of theoretical petal length

$W_{WT}(\lambda) := 2 \cdot W_{tw}(\lambda)$ Total Petalling Work (Wierzbicki & Thomas) as a function of theoretical petal length

For a theoretical petal length of 70mm the force and work are:

$F_{WT}(70 \cdot mm) = 7.733 \times 10^3\ N$ $W_{WT}(70 \cdot mm) = 338.297 J$

And traces of force and work as a function of theoretical petal length:

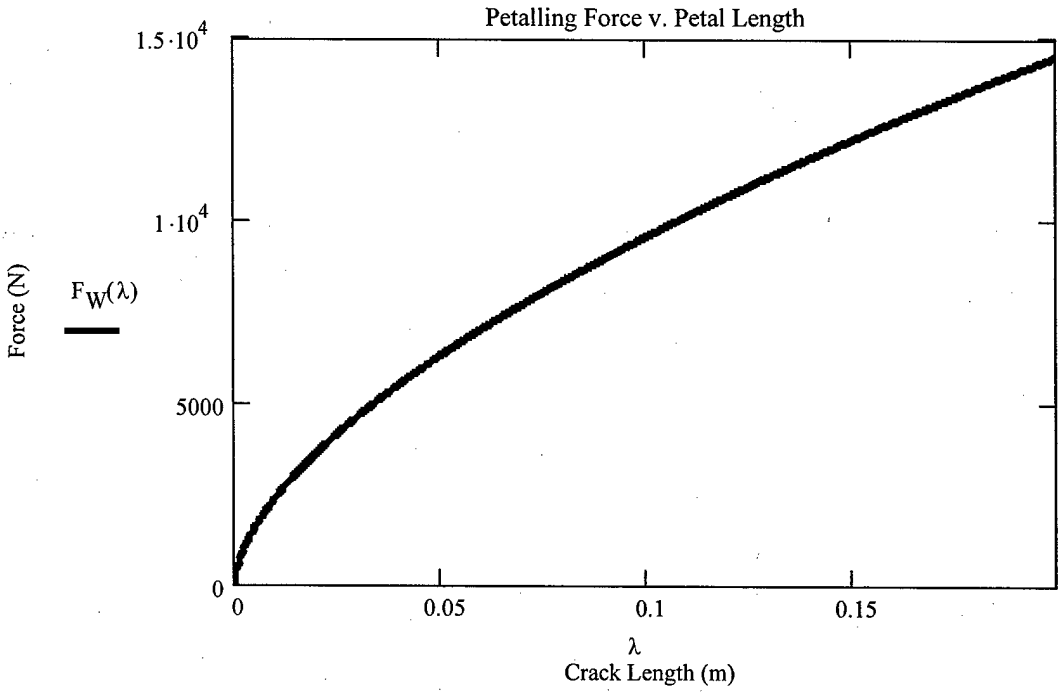
Petalling Force v. Petal Length
1.5·10^4
1·10^4
5000
0
Force (N)
F_W(λ)
0
0.05
0.1
0.15
λ
Crack Length (m)

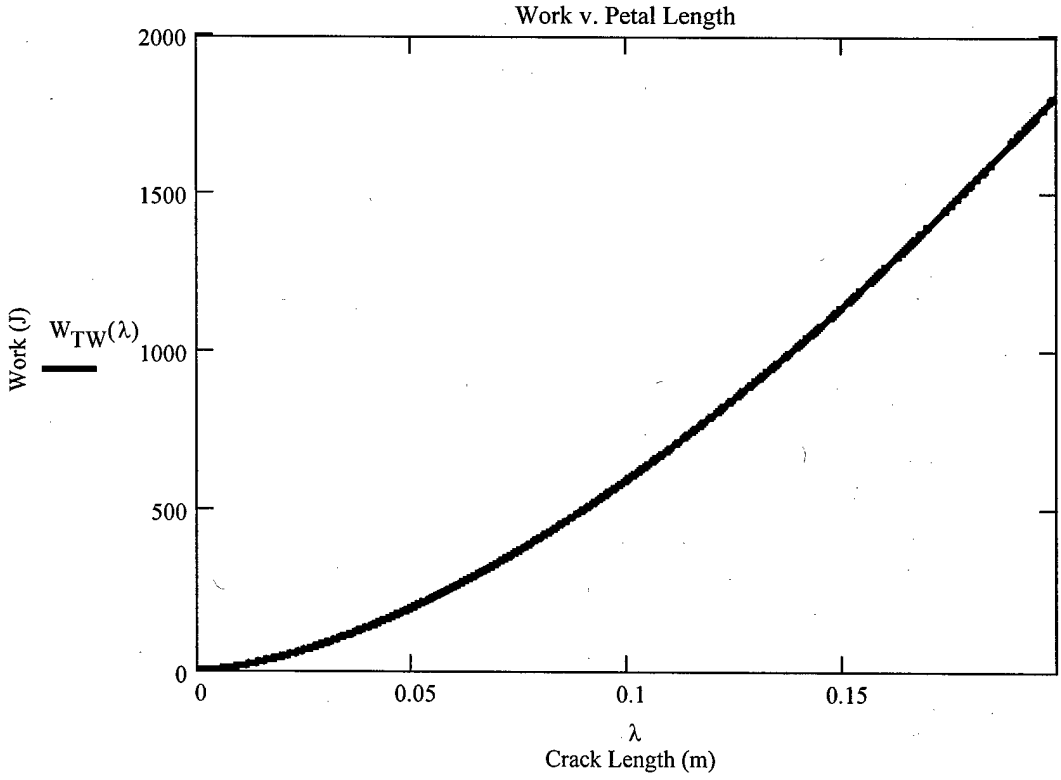
Work v. Petal Length
2000
1500
1000
500
0
Work (J)
W_TW(λ)
0
0.05
0.1
0.15
λ
Crack Length (m)

These results resemble data from many wedge cutting studies. The Force plot indicates that with the application of a small force on the wedge a small cut is initiated, and that there is no threshold force required for the onset of fracture.

For material with the same properties, and with equivalent fracture lengths, it is seen that the wedge derivations of minimum cutting force of Wierzbicki et al. do not compare well with the simplified petalling derivations of Woertz. With respect to force, Woertz's petalling derivations seem much more likely, indicating a minimum force before petalling is initiated and cracks begin to form. The wedge derivations indicate that fracture occurs almost immediately upon application of force.

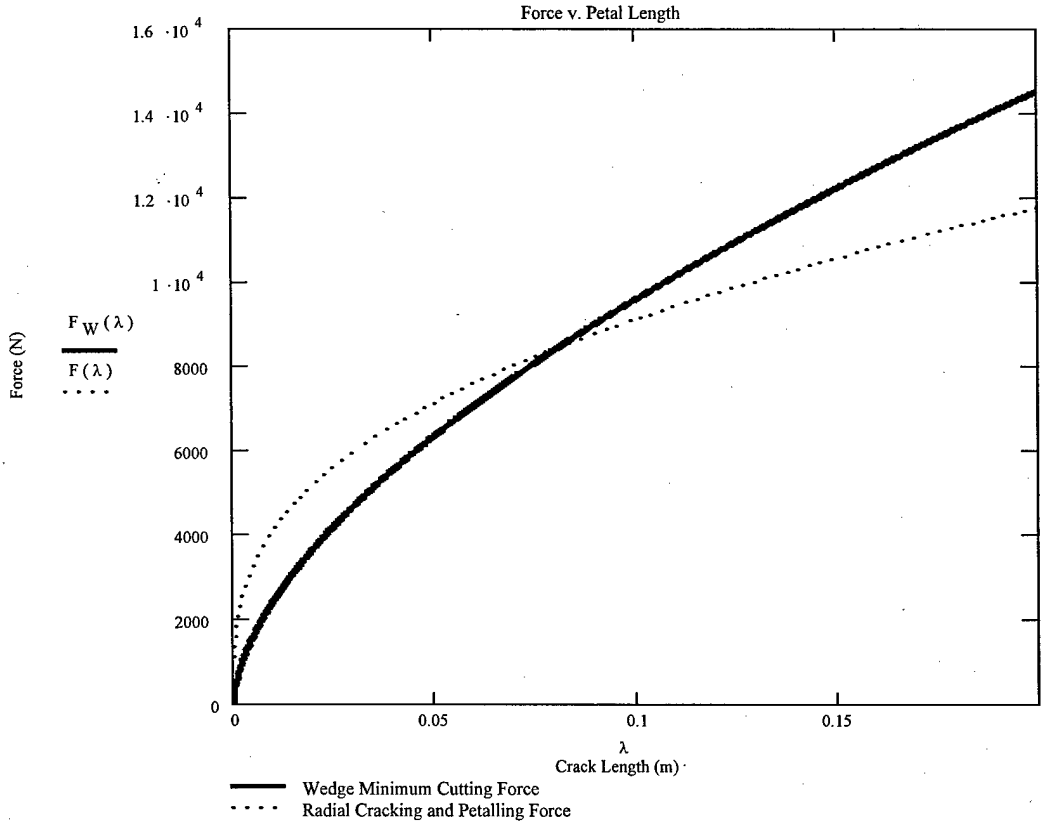

A comparison of the derivations of work dissipated in each case proves to be similar. It is seen that the derivation of work for the wedge cutting and petalling processes compare well, for samples of similar characteristics.

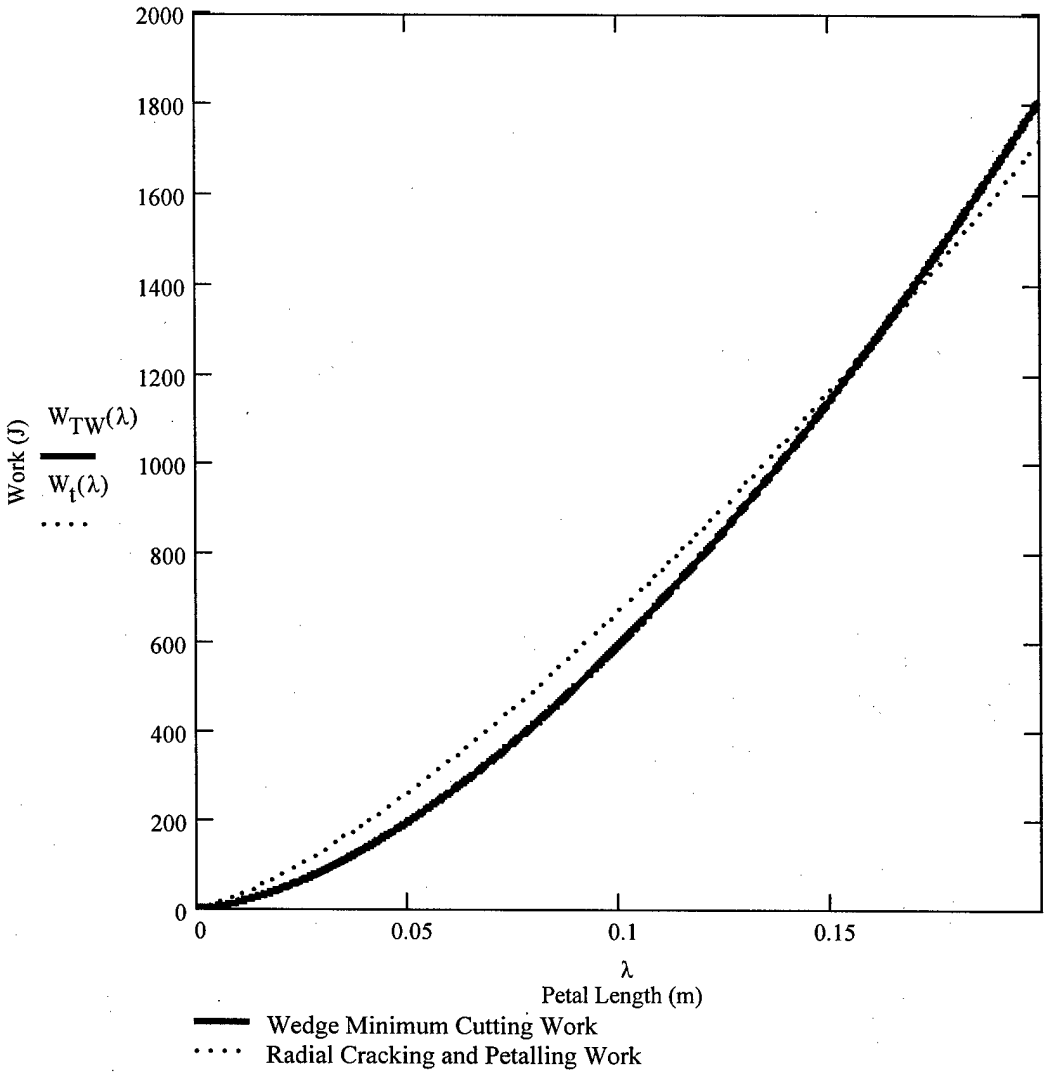
2000
1800
1600
1400
1200
1000
800
600
400
200
0
0
0.05
0.1
0.15
Work (J)
$W_{TW}(\lambda)$
$W_t(\lambda)$
λ
Petal Length (m)
Wedge Minimum Cutting Work
Radial Cracking and Petalling Work

APPENDIX C: TABBING/PETALLING FORCE-DISPLACEMENT APPROXIMATION

For a sample plate of thin, ductile metal with the following characteristics:

$h := .5 \cdot mm$ — Plate thickness

$\sigma_0 := 272 \cdot 10^6 \cdot Pa$ — Average Flow Stress

$\Lambda_0 := 1.5 \cdot cm$ — Pre-cut tab/petal length

$CTOA := 10 \cdot deg$ — Crack tip opening angle (CTOA)

And tab/petalling geometry:

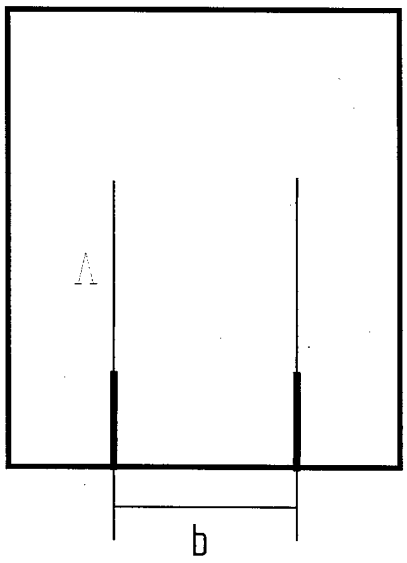

$\theta := 30 \cdot deg$ — Corresponding to petal semi-angle

where n=6

$b := 3 \cdot cm$ Approximately constant tab/petal width

On the testing apparatus with the following characteristics:

$\rho_o := 1.5 \cdot cm$ Rolling cylinder radius

$\rho_{wr} := 3 \cdot cm$ Wire rope cylinder radius

$\Delta_{dot} := 10 \cdot \frac{mm}{min}$ Cross head vertical speed

$\Lambda(\lambda) := \lambda + \Lambda_c$ Total petal length as a function of fracture length

$\lambda(\Delta) := \Delta \cdot \frac{\rho_o}{\rho_{wr}}$ Fracture length as a function of cross-head displacement

Resulting in:

$\Lambda_{dot} := \Delta_{dot} \cdot \frac{\rho_o}{\rho_i}$ Petal length rate of change

$\delta_{ctod}(\lambda) := 2 \cdot \lambda \cdot \sin(CTOA)$ Crack tip opening distance as a function of fracture length

$\delta_{ctod}(\Delta) := 2 \cdot \Delta \cdot \frac{\rho_o}{\rho_{wr}} \cdot \sin(CTOA)$ CTOD as a function of cross-head displacement

Total bending moment per petal per unit length

$M_o := \frac{\sigma_o \cdot h^2}{4}$ $M_o = 17 \frac{N \cdot m}{m}$

$$W_b(\lambda) := \frac{2 \cdot M_o \cdot \left(\Lambda(\lambda) - \Lambda_o\right) \cdot b}{\rho_o}$$

Total bending work per petal as a function of fracture length

$$W_b(\Delta) := \frac{2 \cdot M_o \cdot \left(\Delta \cdot \frac{\rho_o}{\rho_{wr}}\right) \cdot b}{\rho_o}$$

Total bending work as a function of cross-head displacement

And the contribution of membrane work was expressed as:

$$W_m(\lambda) := M_o \cdot \left(\Lambda(\lambda) - \Lambda_o\right) \cdot 3.84 h^{-1} \cdot \left(\delta_{ctod}(\lambda)\right)^{\frac{1}{3}} \cdot (\rho_o)^{\frac{2}{3}} \cdot \sin(\theta)^{\frac{-4}{3}} \cdot \cos(\theta)^{-1}$$

or:

$$W_m(\Delta) := M_o \cdot \left(\Delta \cdot \frac{\rho_o}{\rho_{wr}}\right) \cdot 3.84 h^{-1} \cdot \left(\delta_{ctod}(\Delta)\right)^{\frac{1}{3}} \cdot (\rho_o)^{\frac{2}{3}} \cdot \sin(\theta)^{\frac{-4}{3}} \cdot \cos(\theta)^{-1}$$

Making the total work:

$$W_t(\Delta) := W_m(\Delta) + W_b(\Delta)$$

And the total force:

$$F(\Delta) := \frac{d}{d\Delta} W_t(\Delta)$$

Traces of force and work as a function of cross-head displacement:

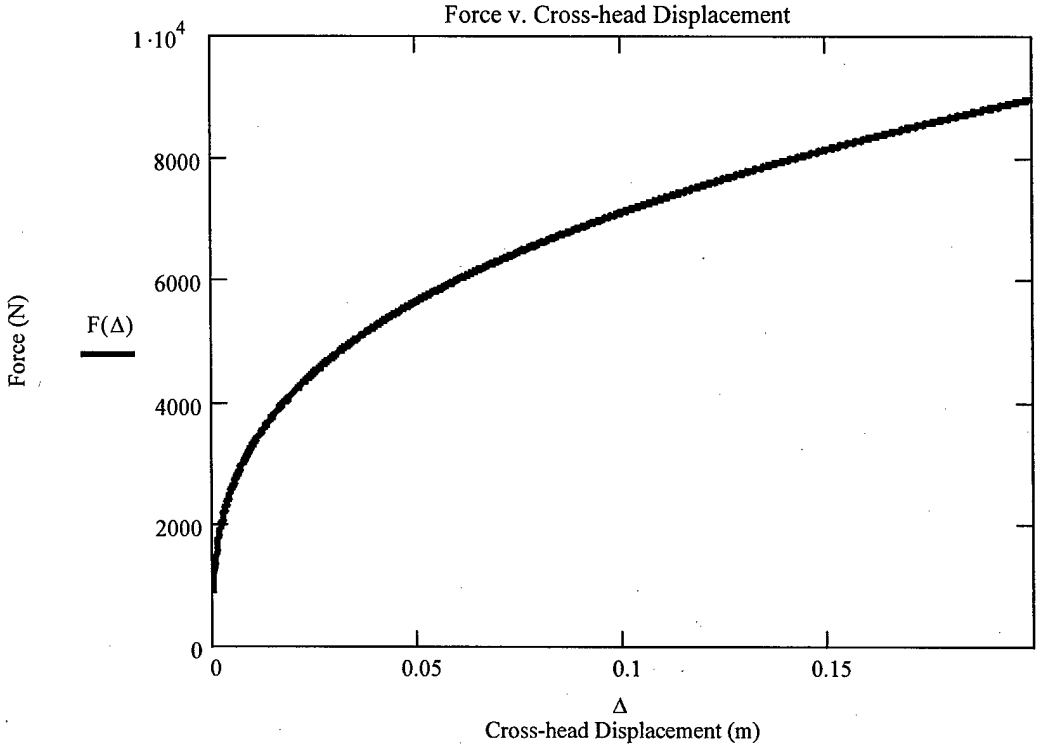

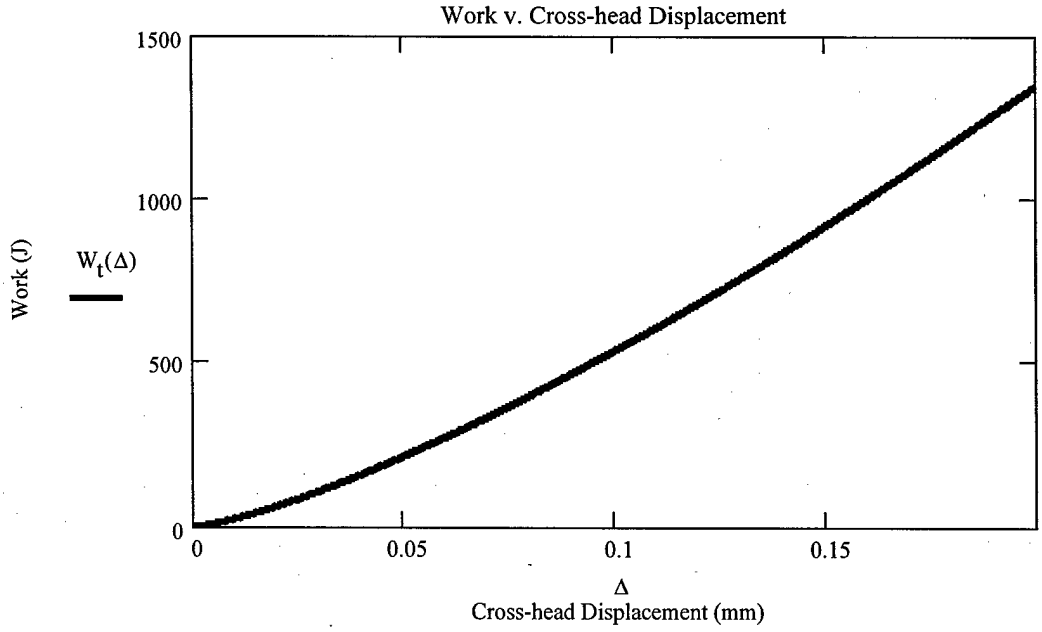

APPENDIX D – PHASE ONE: SAMPLE GEOMETRY TEST RESULTS

Sample 1: n=4, Triangular Tab

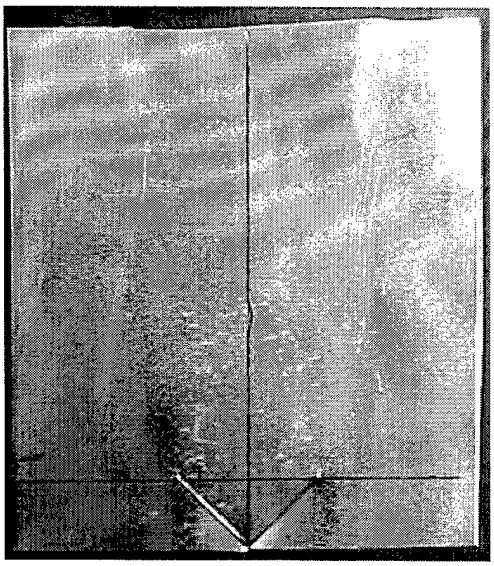

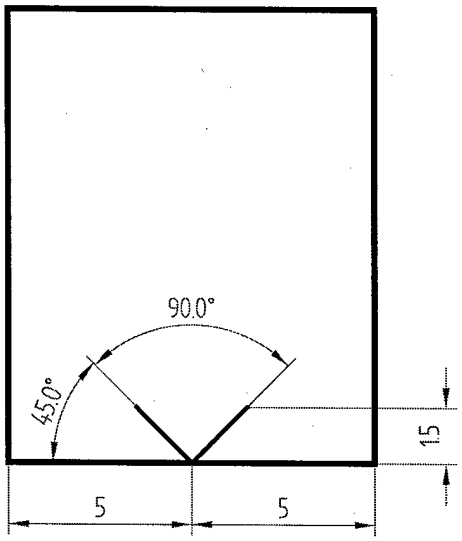

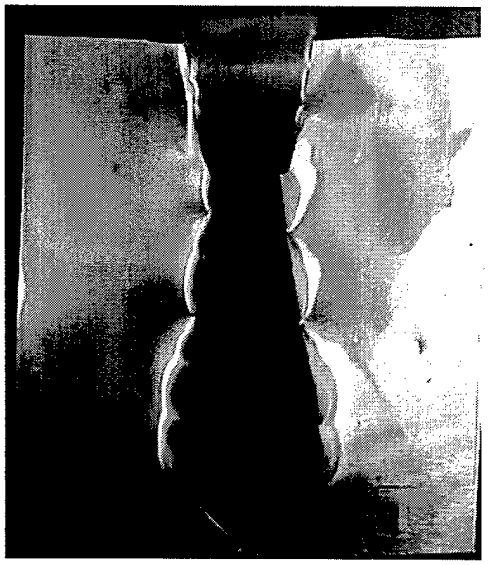

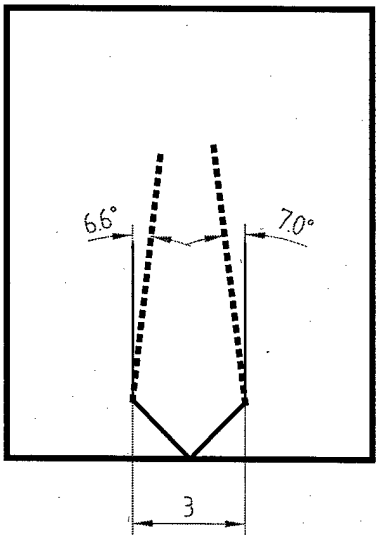

- Converging fracture geometry
- Average angle of convergence=6.8 degrees
- Effective Fracture Length=80mm (Maximum)

Sample 2: n=4, Trapezoidal Tab

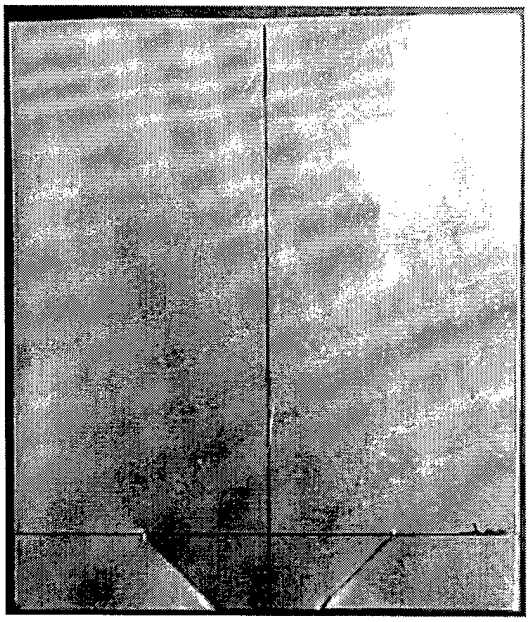

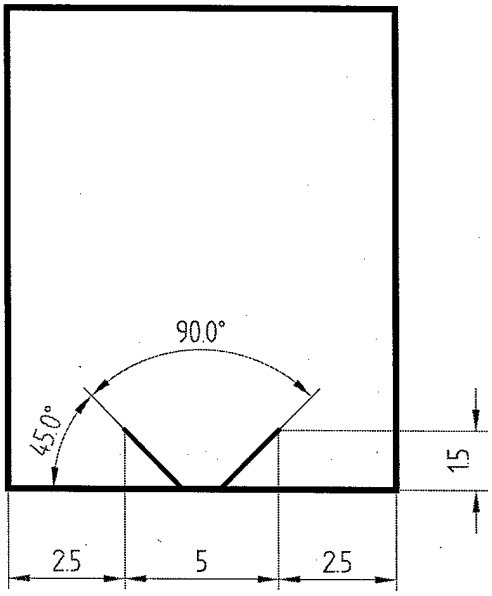

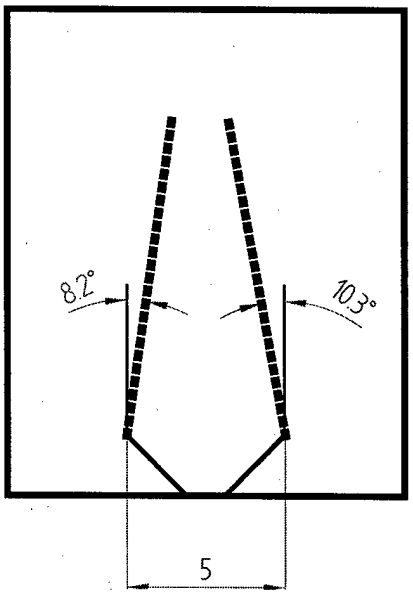

- Converging fracture geometry
- Average angle of convergence=9.25 degrees
- Effective Fracture Length=80mm (Maximum)

Sample 3: n=6, Triangular Tab

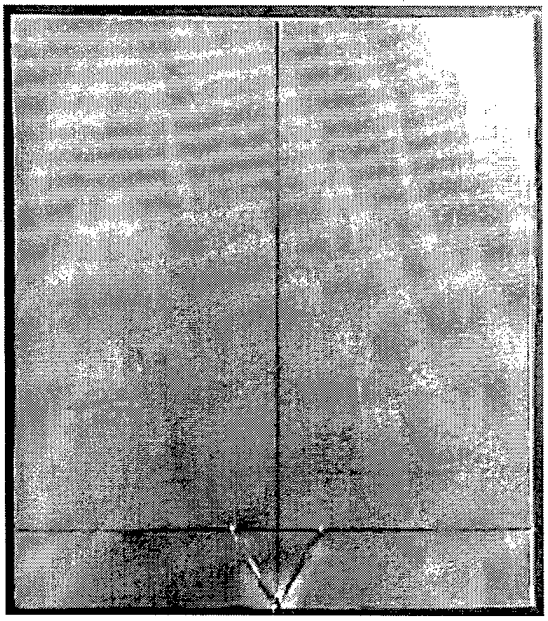

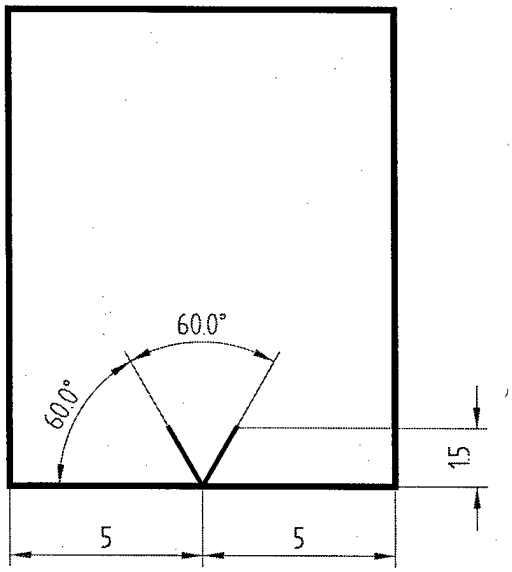

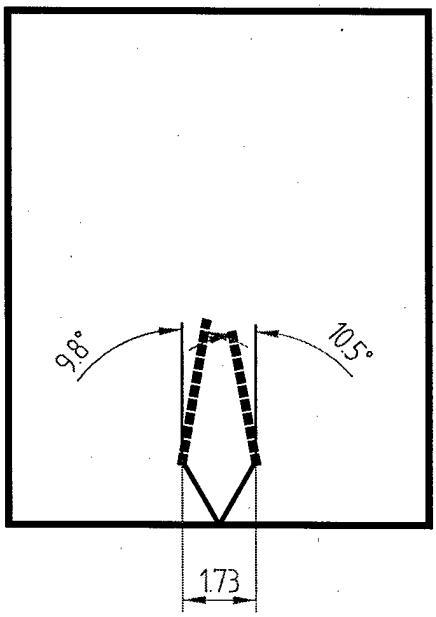

- Converging fracture geometry
- Average angle of convergence=10.15 degrees
- Effective Fracture Length=41mm

Sample 4: n=6, Trapezoidal Tab

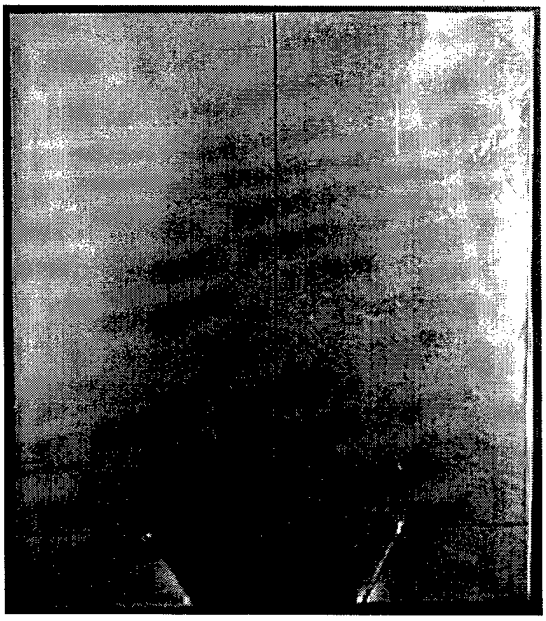

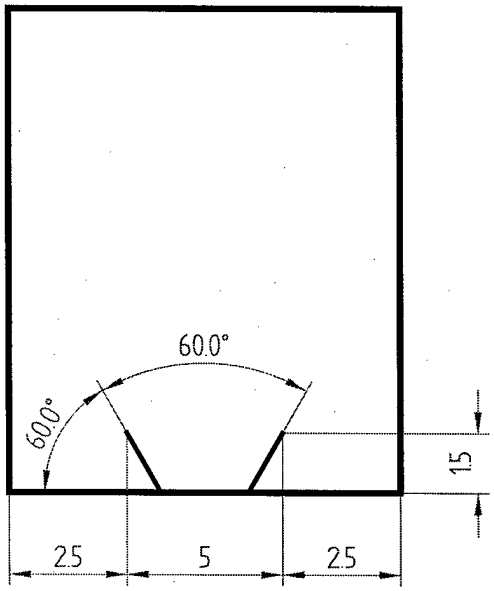

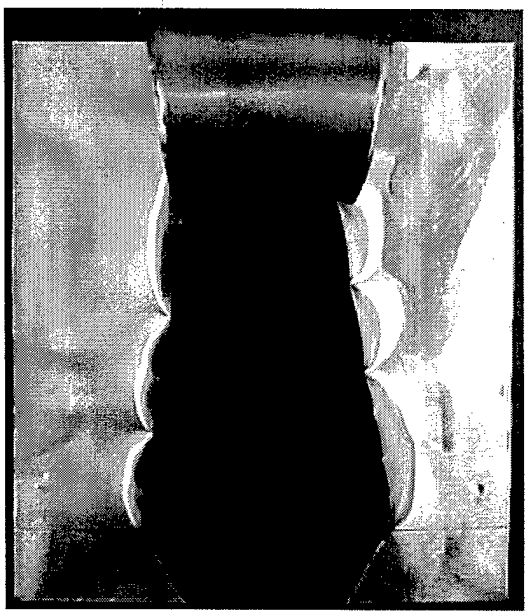

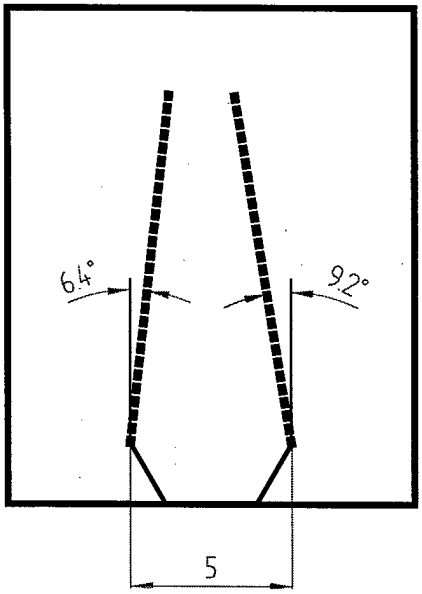

- Converging fracture geometry
- Average angle of convergence=7.8 degrees
- Effective Fracture Length=80mm (Maximum)

Sample 5: Rectangular Tab

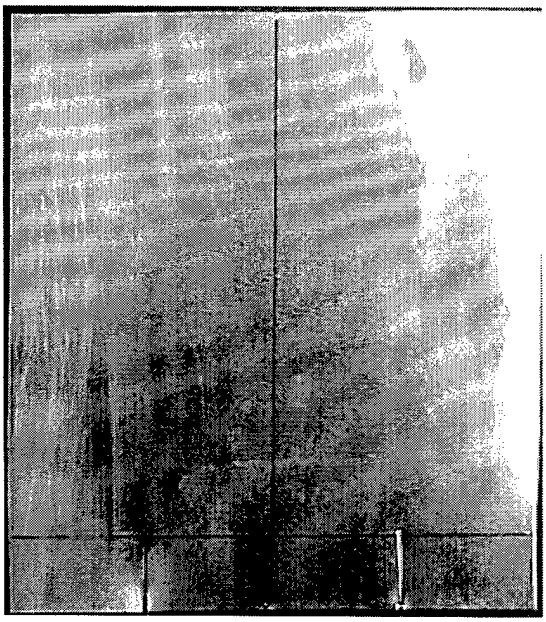

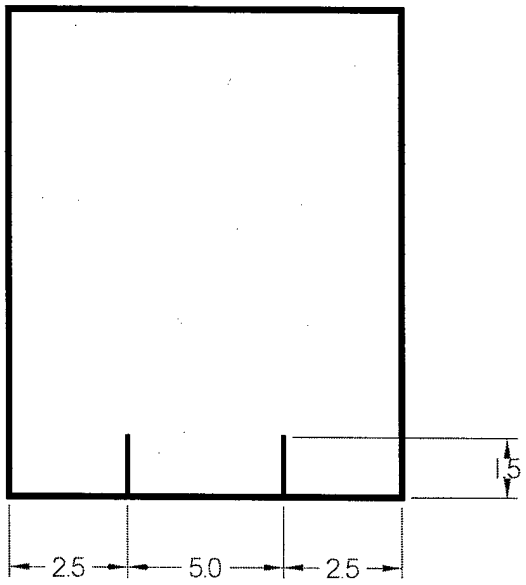

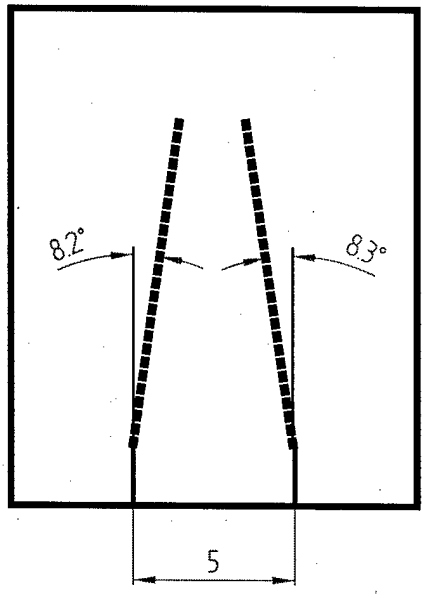

- Converging fracture geometry
- Average angle of convergence=8.25 degrees
- Effective Fracture Length=80mm (Maximum)

APPENDIX E – MATERIAL SAMPLE SPECIFICATIONS AND GEOMETRY

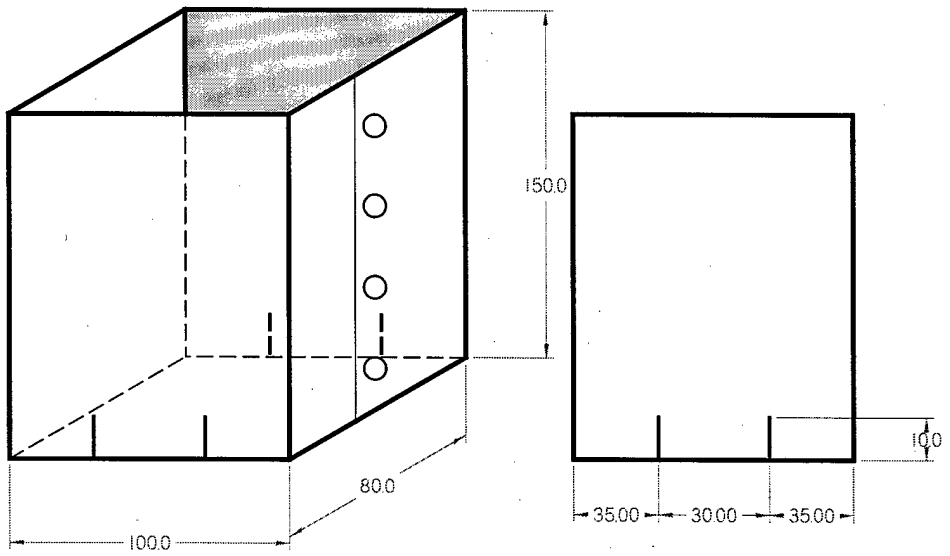

90 degree bends

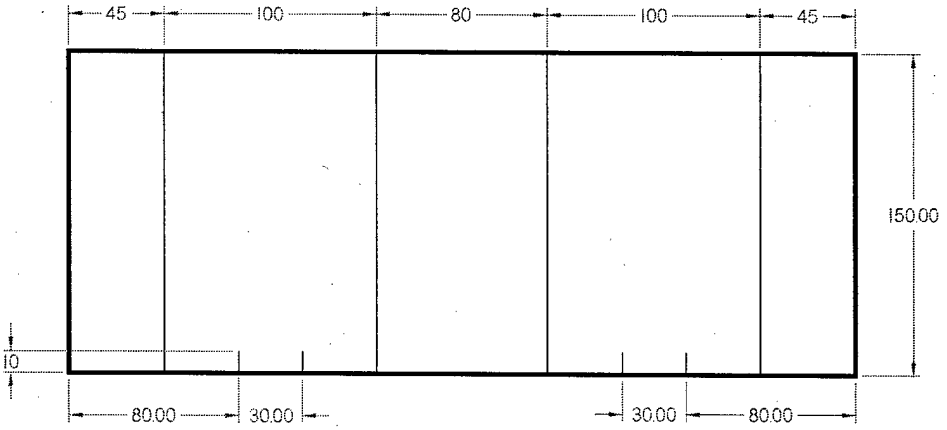

Sample Tensile Test Results

0.711mm Thickness Sample

0.406mm Thickness Sample

APPENDIX F – PHASE TWO: TEST APPARATUS GEOMETRY TEST RESULTS

Flush Mounted Geometry

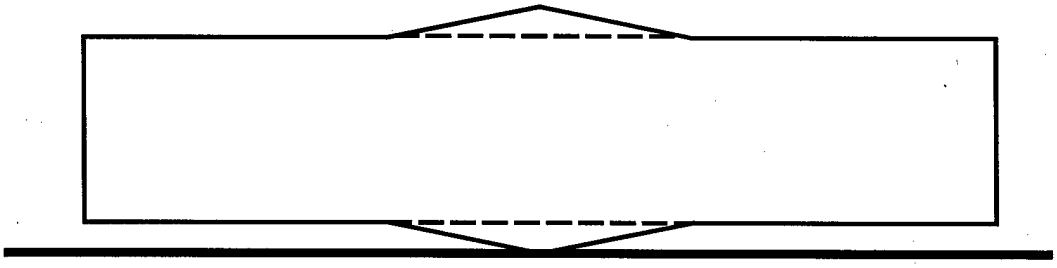

Sample 1: Parallel Cylinder, 15mm Radius

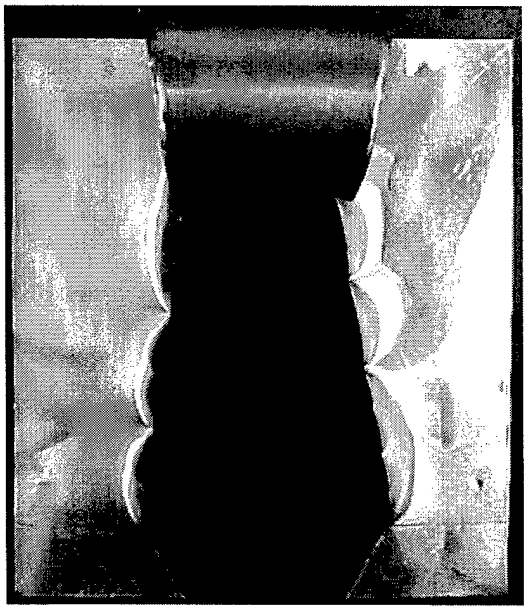

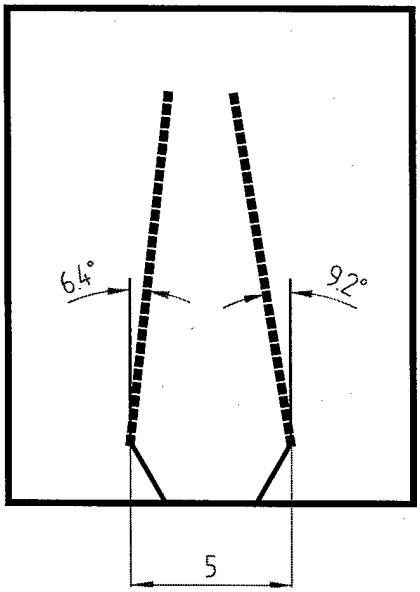

- Average angle of convergence=7.8 degrees

Sample 2: Conically Tapered, 20mm Maximum Radius

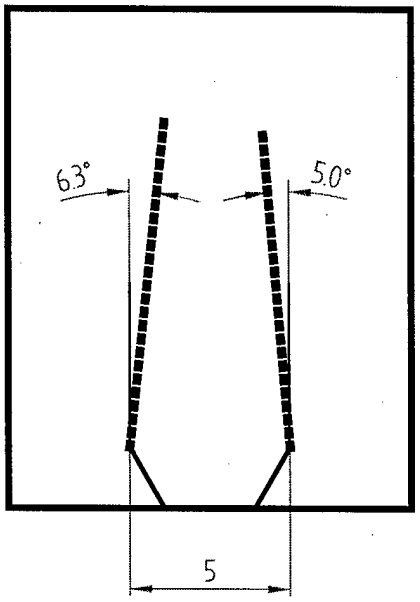

- Average angle of convergence=5.65 degrees

Sample 3: Spherically Tapered, 20mm Maximum Radius

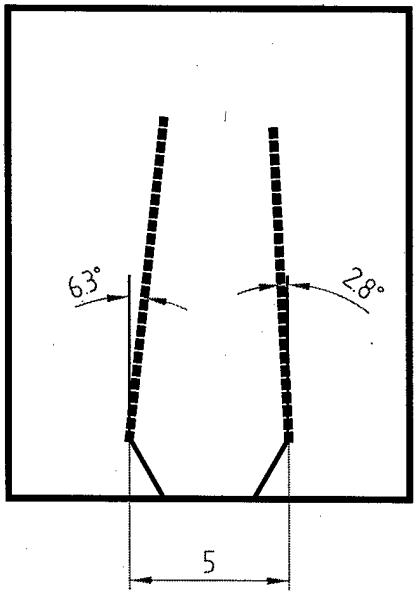

- Average angle of convergence=4.55 degrees

Recess Mounted Geometry

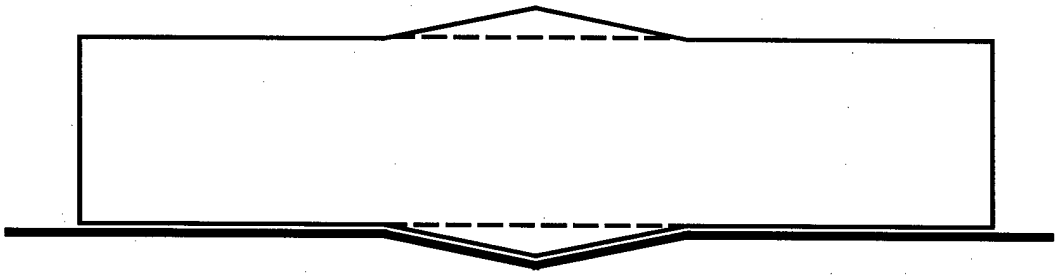

Sample 4: Conically Tapered, 20mm Maximum Radius

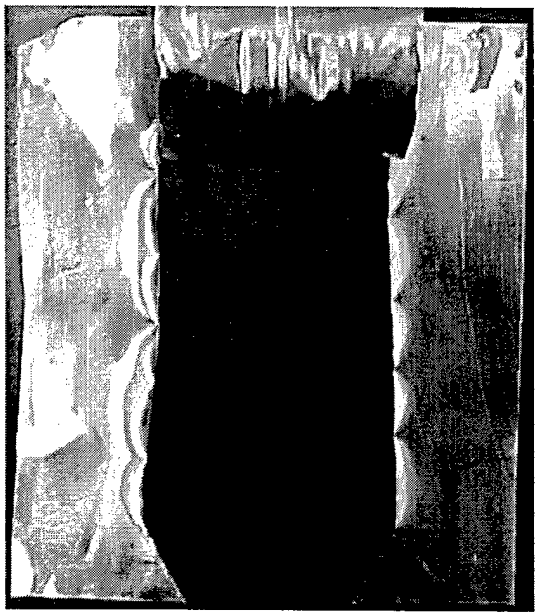

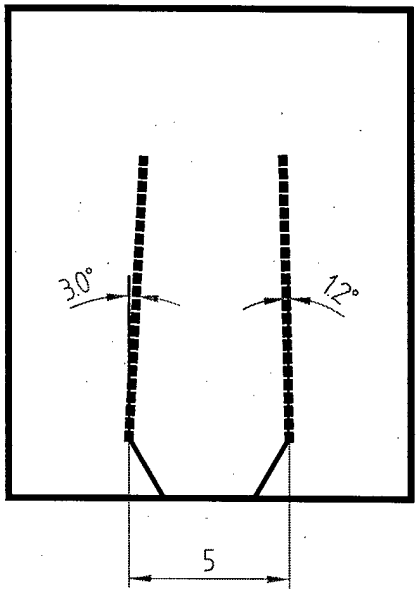

- Average angle of convergence=2.1 degrees

Sample 5: Spherically Tapered, 20mm Maximum Radius

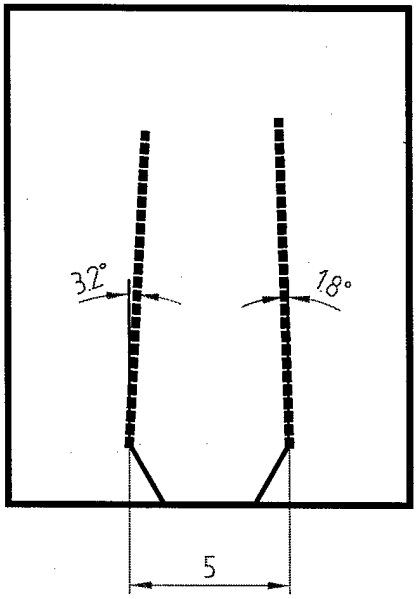

- Average angle of convergence=2.5 degrees

APPENDIX G – APPARATUS DESIGN, GEOMETRY AND SPECIFICATIONS

Design Details

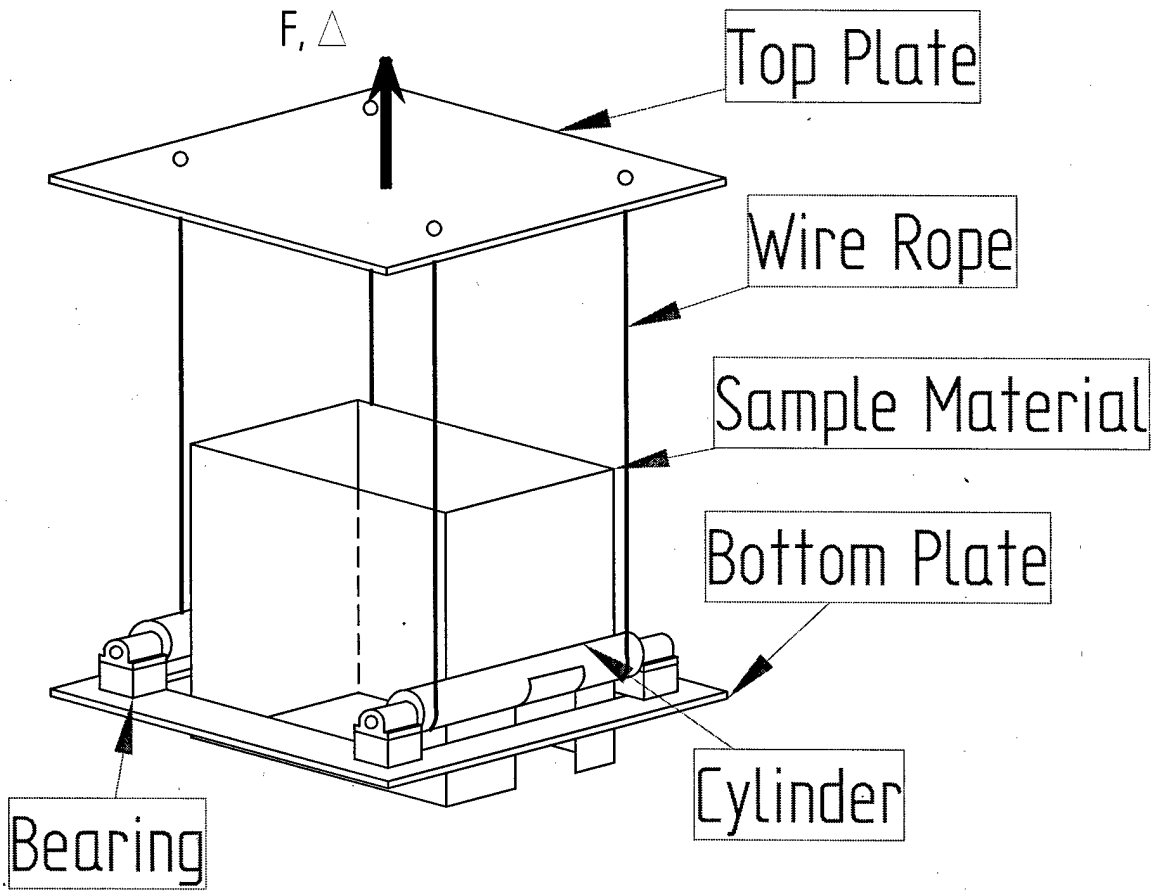

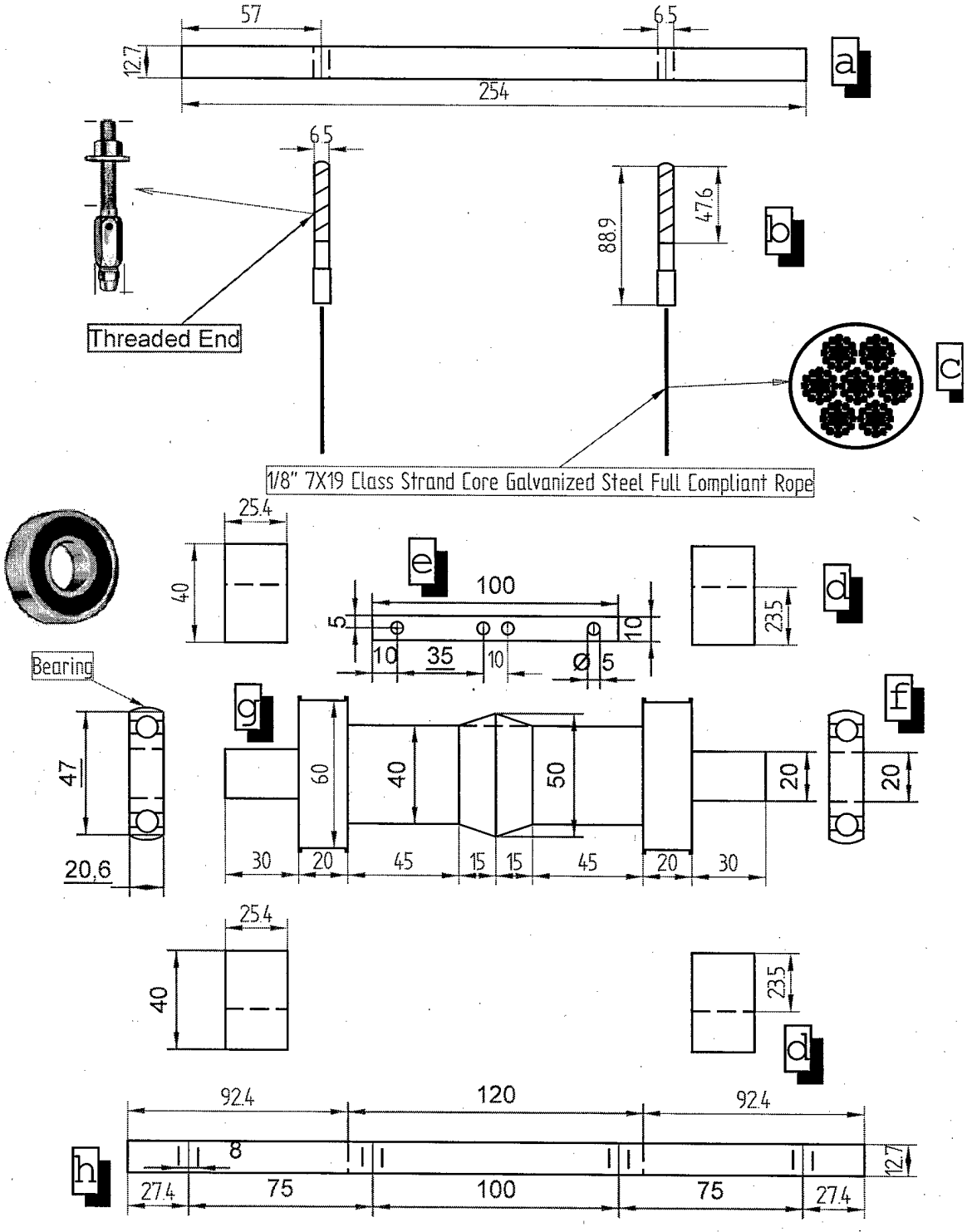
57
6.5
12.7
254
a
6.5
Threaded End
88.9
47.6
b
c
1/8" 7X19 Class Strand Core Galvanized Steel Full Compliant Rope
25.4
40
e
100
5
10
10
35
10
Ø 5
d
23.5
Bearing
47
20.6
g
60
40
50
20
20
f
30
20
45
15
15
45
20
30
25.4
40
23.5
d
92.4
120
92.4
h
8
12.7
27.4
75
100
75
27.4

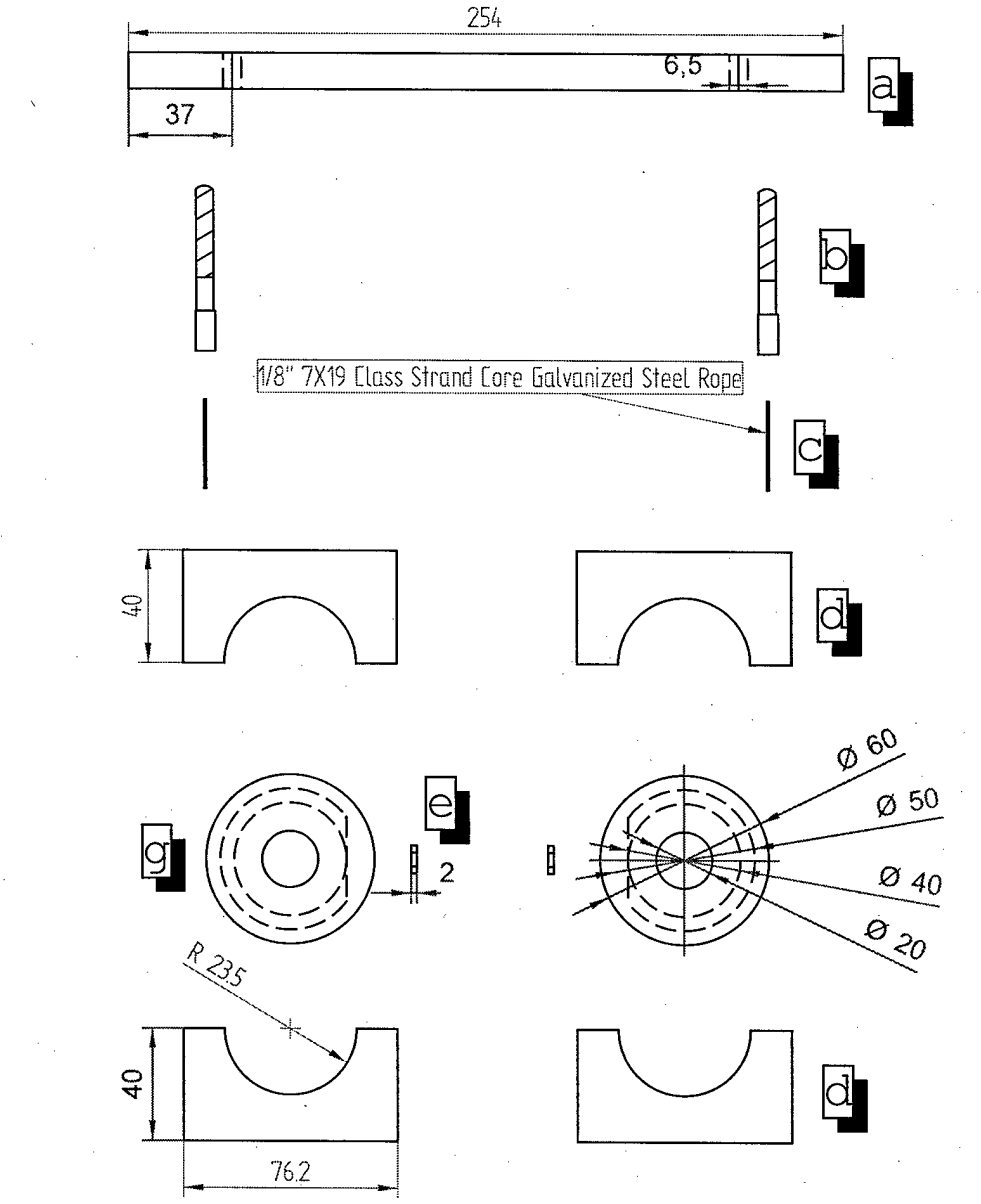
254
6,5
37
a
b
1/8" 7X19 Class Strand Core Galvanized Steel Rope
c
40
d
e
g
2
Ø 60
Ø 50
Ø 40
Ø 20
R 235
40
76.2
d
h
8
12.7
27.4
75
100
75
27.4

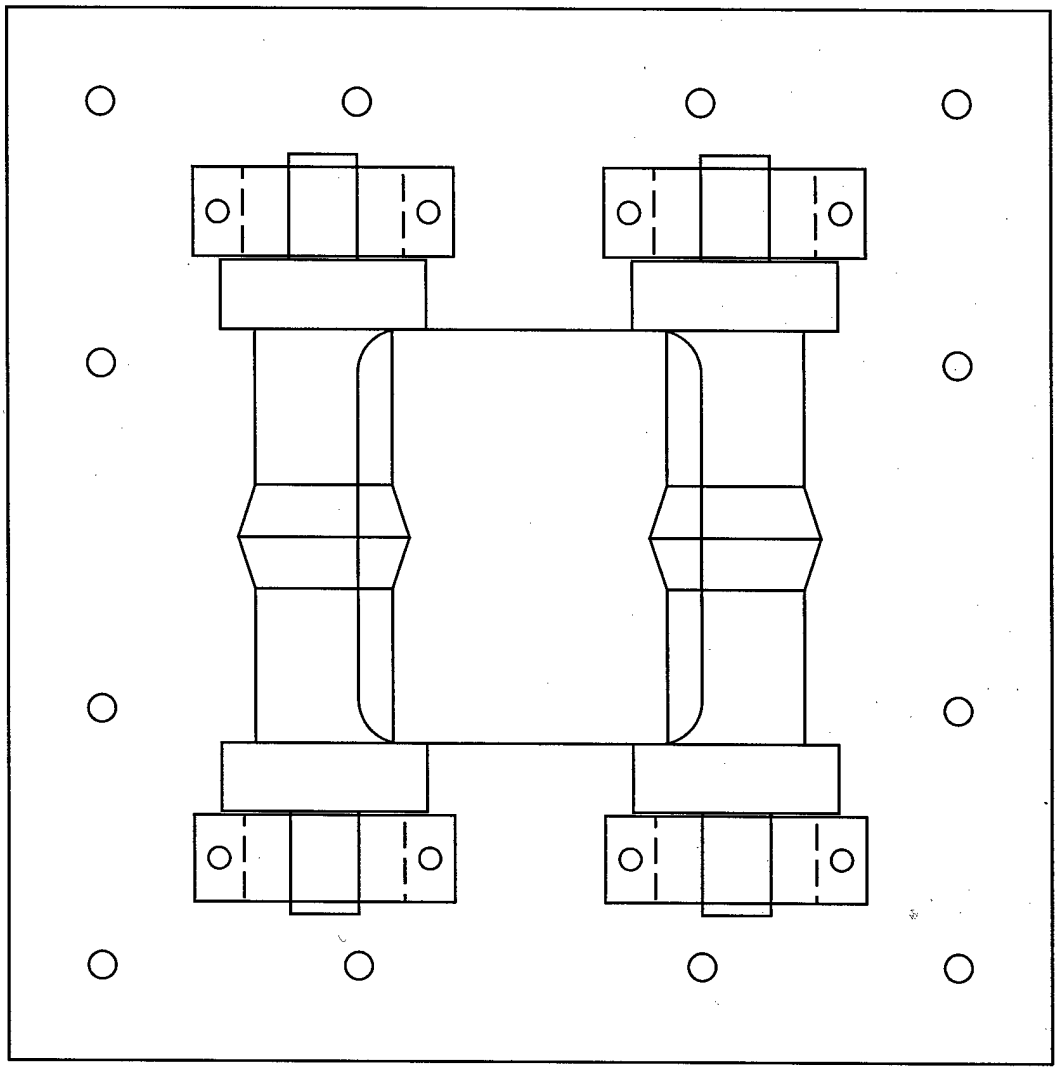

100 KSI Tension Yield Tooled Steel

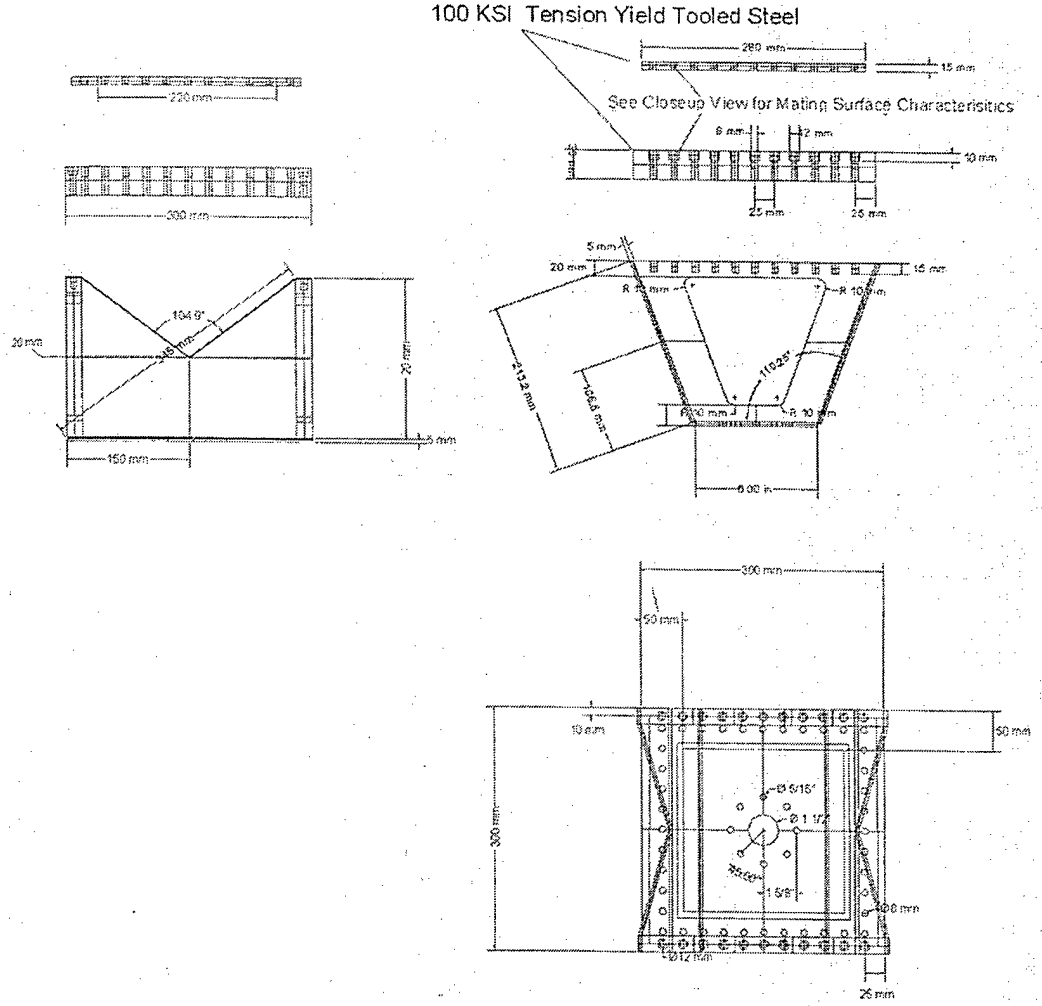

Component Specifications

a -- Top Plate

C-1018 Low Carbon Steel – 10inX10inX0.5in. Conforms to ASTM A108. Heat-treating, in contact with carbon (carburizing), hardens the surface of this low-carbon steel. It is easy to cold form, bend, braze, and weld. Maximum attainable Rockwell hardness is B72. Melting point is 2800 F. Yield strength is 55,000psi. Cold finished. Width and length tolerances are ±0.125in. Thickness tolerance is ±0.003in.

b -- Threaded Adjustment End

Plain Steel Positive Grip Wire Rope End Fittings. Fitted with 0.25in., 28 thread, end details.

c -- Wire Rope

Galvanized Steel Multi-Purpose Rope—7×19 class strand core commercial grade. Unlubricated rope offers a good balance of strength and flexibility in diameters less than 1/8in. It is stronger but less flexible than six-strand core constructions.

7 x 19 Class Strand Core

Galvanized wire rope has a zinc coating that provides added corrosion protection. In mild environments, it's an economical alternative to stainless steel. The strength of galvanized rope is generally less than that of plain steel and stainless steel. 0.125in diameter and 2000lb. Breaking strength. Meets specifications:

- Fed. Spec. RR-W-410
- Breaking Strength of Mil-DTL-83420

This wire rope displays the following linear load-extension characteristics:

Load = Percent Strain * Modulus

where:

Modulus=1190.25 pounds per percent extension

d -- Pillow Block Assembly

C-1018 Low Carbon Steel Precision Ground Stock. Conforms to ASTM A108. Heat-treating, in contact with carbon (carburizing), hardens the surface of this low-carbon steel. It is easy to cold form, bend, braze, and weld. Maximum attainable Rockwell hardness is B61-B62. Melting point is 2800 F. Yield strength is 55,000psi. Cold finished. Width and length tolerances are +0.005in. Thickness tolerance is ±0.001in.

e -- Sample Fastener Bar

f -- Double-Row Ball Bearings

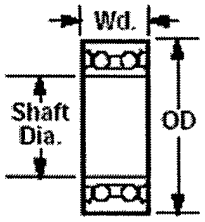

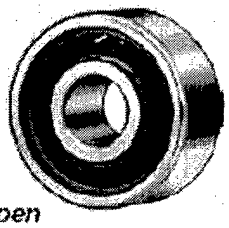
Open

Double-Row, Double Shielded Steel Ball Bearing – ABEC-1. Double-row ball bearings handle high radial loads. The balls are held in place at 25° angles between the inner and outer sleeves. They're ideal for pumps, gear motors, and large electric motors. Temperature range is -40° to +250° F. Double-shielded bearings have steel shields that help keep out dirt and preserve lubricants. Shaft diameter 20mm. Outside Diameter 47mm. Width 20.6mm. Maximum dynamic radial load 4450lb. Maximum RPM 10000.

g -- Tapered Cylindrical Roller

12L14 Carbon Steel Rod. Conforms to ASTM A108. Low-carbon steel that has excellent machining characteristics and good ductility making it easy to bend, crimp, and rivet. It is very difficult to weld and cannot be case hardened. Maximum attainable Rockwell hardness is B75-B90. Melting point is 2800° F. Yield strength is 60,000-80,000psi. Cold drawn.

h -- Base Plate

C-1018 Low Carbon Steel – 12inX12inX0.5in. Conforms to ASTM A108. Heat-treating, in contact with carbon (carburizing), hardens the surface of this low-carbon

steel. It is easy to cold form, bend, braze, and weld. Maximum attainable Rockwell hardness is B72. Melting point is 2800 F. Yield strength is 55,000psi. Cold finished. Width and length tolerances are ±0.125in. Thickness tolerance is ±0.003in.